

The mean square radius of the neutron distribution in the relativistic and non-relativistic mean field models

Haruki Kurasawa^{1*} and Toshio Suzuki^{2†}

¹ Department of Physics, Graduate School of Science, Chiba University,
Chiba 263-8522, Japan

² Research Center for Electron Photon Science, Tohoku University,
Sendai 982-0826, Japan

It is investigated why the root mean square radius of the point neutron distribution is smaller by about 0.1 fm in non-relativistic mean field models than in relativistic ones. The difference is shown to stem from the different values of the product of the effective mass and the strength of the one-body potential in the two frameworks. The values of those quantities are constrained by the Hugenholtz-Van Hove theorem. The neutron skin is not a simple function of the symmetry potential, but depends on the nucleon effective mass.

1 Introduction

Recently much has been written on the neutron distribution in nuclei[1, 2, 3, 4, 5]. It is one of the most fundamental problems in nuclear physics together with the proton distribution[1, 6]. The neutron distribution, however, has not been well determined experimentally so far. This fact is because the neutron density has been studied through hadron probes, where the ambiguity as to the interaction and the reaction mechanism is not avoidable yet[3].

In contrast to the neutron distribution, the proton distribution is widely investigated throughout the periodic table of the stable nuclei theoretically[6] and experimentally[7]. The relationship between the point proton and charge density distributions is defined unambiguously[6, 8]. The latter is deduced from electron scattering cross sections rather model-independently[7], compared with the strong interaction, since the electromagnetic interaction is well understood, and is so weak that the density distribution of the nuclear ground state is not disturbed[6, 9].

It has been believed for a long time that electron scattering is useless in the study of the neutron distribution in nuclei[6, 10]. Recently, the present authors have proposed a new way to deduce the neutron distribution from electron scattering data[8]. They have derived the exact expression of the n th-order moment of the nuclear charge distribution, and shown that the mean square radius(msr) of the charge distribution(R_c^2) is dominated by the msr of the point proton distribution(R_p^2) and is independent of the neutron's msr(R_n^2), but that the n th-order ($n \geq 4$) moment of the charge density depends on the $(n-2)$ -order moment of the neutron distribution[8]. For example, the fourth-order moment of the charge density(Q_c^4) depends on R_n^2 . Their relationship is uniquely defined, and the value of Q_c^4 is well determined in electron scattering experiment[7, 11]. The value of R_n^2 , however, is not separated from Q_c^4 experimentally. In order to deduce the value of R_n^2 from the experimental value of Q_c^4 , it is necessary to rely on a model-dependent analysis.

At present, the nuclear structure is not investigated without invoking phenomenological models. Moreover, most of the models are constructed for different purposes independently.

*kurasawa@faculty.chiba-u.jp

†kt.suzuki2th@gmail.com

Hence, it is not appropriate for the separation of R_n^2 from Q_c^4 to choose one model among many existing models. The present authors[4] have proposed the least squares analysis(LSA) for the separation by employing as many previous models as possible together. Through the LSA, they explore the constraints which are inherent in the framework of the nuclear models. The procedure of the separation is as follows. First R_n^2 and Q_c^4 are calculated using several models in the same framework, and then the least square line(LSL) for those values is obtained in the $R_n^2 - Q_c^4$ plane. Next, the value of R_n^2 in the framework is determined by the cross point of the LSL and the line of Q_c^4 corresponding to its experimental value. In order to confirm the obtained result, the LSA of R_n^2 against the other moments also has been performed. The estimated values of R_n^2 are not model-independent, but are derived on the basis of the data from the well-known electromagnetic probe, with utilizing the knowledge on the phenomenological models accumulated for a long time in nuclear physics. A similar method has been proposed for analyzing the parity violating electron scattering[2], and employed actually in the analysis of the recent JLab experiment[5, 12].

In the Ref.[4], the values of R_n^2 in ^{40}Ca , ^{48}Ca and ^{208}Pb have been estimated, for which the experimental values of Q_c^4 are available at present. They have arbitrarily chosen 11 relativistic and 9 non-relativistic models among more than 100 versions accumulated for the last 50 years[13, 14, 15, 16]. Those models well reproduce fundamental nuclear properties within the mean field framework, assuming some nuclei to be a double closed shell nucleus. The LSL is obtained with a small standard deviation and the values of R_n^2 are determined within the 1% error including experimental one[4]. In this analysis, it has been shown that the relativistic and non-relativistic frameworks yield different values of R_n^2 from each other in ^{48}Ca and ^{208}Pb . The value of R_n in the non-relativistic models is smaller by about 0.1 fm than that in the relativistic models in both nuclei. Since in those mean field models, the values of R_p are fixed so as to reproduce the experimental values, the neutron skin defined by $\delta R = R_n - R_p$ differs by about 0.1 fm in the two frameworks. The difference is not between each models, but between the two frameworks, so that the result is apparently understood to reflect an essential difference between the structures of the two mean field approximations.

It should be noted that the 0.1 fm is not small for the neutron skin itself. As seen later, for example, in ^{208}Pb , δR is 0.275 and 0.162 fm in the relativistic and non-relativistic models, respectively. Understanding the 0.1 fm difference may be important for the study of nuclear fission and fusion phenomena which are sensitive to the structure of nuclear surface[1, 17]. Recent detailed calculations[18] may not neglect order of 0.1 fm difference in describing asymmetric nuclei. The 0.1 fm difference has been pointed out to be crucial for the neutron star physics also[3, 18].

The purpose of the present paper is to investigate why the values of R_n^2 in the non-relativistic mean field models is smaller than in the relativistic ones. The difference will be shown to stem mainly from the difference between the products of the effective mass and the strength of the one-body potential in the two frameworks. These two quantities are constrained in each framework by Hugenholtz-Van Hove(HVH) theorem[19, 20, 21]. The theorem has been proved in the mean field approximation in the non-relativistic framework for the symmetric nuclear matter. As will be shown in the present paper, the theorem holds in the asymmetric nuclear matter in both relativistic and non-relativistic models, and is numerically maintained in the mean field approximation for finite nuclei also.

In §2, the root msr R in the one-body potential will be discussed in order to derive an

analytical expression of R in terms of the strength of the potential and the nucleon effective mass, using the Woods-Saxon and harmonic potentials. In §3, the equations of motion in the relativistic models will be shown to have the same structure as the Schrödinger equation in the non-relativistic models. In §4, the HVH theorem will be extended to asymmetric nuclear matter. In §5, the complexity of the mean field models due to a large variety of interaction parameters will be simplified by using the Woods-Saxon type function, aiming to make clear the difference between the relativistic and non-relativistic model. In §6, the difference between δR 's in the two frameworks will be investigated in detail, according to the HVH theorem. The final section will be devoted to a brief summary of the present paper.

2 The nuclear radius in the one-body potential

Many phenomenological models have been proposed with various interaction parameters[13, 16]. The nuclear radius, R , may be a complicated function of their parameters, and the function would be different from one model to another. The radius, however, is one of the most fundamental quantities which determine the structure of the nucleus, and, hence, R_p is used as an input to fix the free parameters of the models. This fact implies that the relationship of R to other key quantities of nuclei like those in the one-body potential must be almost the same in the mean field models, although those key quantities also may depend on the parameters in complicated ways.

Such relationships of R to other key quantities should hold even in simplified one-body potential models, if they well describe the gross properties of nuclei[1]. As a simple one, Woods-Saxon potential(Ws) is most widely used in the literature[1]. It may become a guide for the present purpose also, if we have an analytical formula for relationship between R and the parameters of the one-body Hamiltonian with WS,

$$H = \frac{\mathbf{p}^2}{2M} + V_{\text{ws}}(r), \quad V_{\text{ws}}(r) = \frac{V_{\text{ws}}}{1 + e^{(r-R_{\text{ws}})/a_{\text{ws}}}}. \quad (1)$$

Aiming to have an analytical expression of the relationship, we require the help of the harmonic oscillator potential(HO),

$$V_{\text{H}}(r) = \frac{k}{2} (r^2 - R_{\text{H}}^2), \quad k = M\omega^2, \quad (2)$$

R_{H} being a constant which determines the value of $V_{\text{H}}(0)$. Bohr and Mottelson have shown that the single-particle wave functions in WS, which determine the value of R , are well reproduced by those of HO[1]. In HO, the dimension analysis yields the expression of the radius R_{ho} as

$$R_{\text{ho}} = \frac{C}{(Mk)^{1/4}} \quad (3)$$

with C denoting a constant. For the above exact formula, let us search for the expression of R_{ho} in terms of the WS parameters by minimizing the following quantity with respect to the variables, k and R_{H} ,

$$F_n(k, R_{\text{H}}) = \int_0^{R_{\text{H}}} dr r^n (V_{\text{H}}(r) - V_{\text{ws}}(r))^2, \quad (4)$$

where n is considered to be 0 for the surface integral and 2 for the volume integral. The value of n is chosen by referring to Ref.[1], where $\omega = 8.6$ MeV and $V_{\text{H}}(0) = -55$ MeV are used for $V_{\text{ws}} = -50$ MeV, $R_{\text{ws}} = 5.8$ fm and $a_{\text{ws}} = 0.65$ fm. The numerical method yields the minimum

values of F_n for the same WS parameters at $\omega = 8.63$ MeV and $V_H(0) = -55.20$ MeV for $n = 0$, and at $\omega = 9.66$ MeV and $V_H(0) = -62.65$ MeV for $n = 2$. Comparing these values with those in Ref.[1], it may be reasonable to employ $n = 0$, rather than $n = 2$, for reproducing the wave functions in WS.

Once we determine the value of n , it is possible to derive the analytical formula for the approximate relationship between R_{ho} and the WS parameters. Eq.(4) for $n = 0$ is written as

$$F_0(k, R_H) = \int_0^{R_H} dr \left(V_H(r) - V_{ws}(r) \right)^2 = \frac{2}{15} k^2 R_H^5 + F_H + F_V,$$

where we have defined

$$F_H = -2 \int_0^{R_H} dr V_H(r) V_{ws}(r) = -k V_{ws} \int_0^\infty dr \frac{r^2 - R_H^2}{1 + e^{(r-R_{ws})/a_{ws}}} + \delta F_H, \quad (5)$$

$$F_V = \int_0^{R_H} dr V_{ws}^2(r) = V_{ws}^2 \int_0^\infty \frac{dr}{(1 + e^{(r-R_{ws})/a_{ws}})^2} + \delta F_V, \quad (6)$$

with

$$\delta F_H = k V_{ws} \int_{R_H}^\infty dr \frac{r^2 - R_H^2}{1 + e^{(r-R_{ws})/a_{ws}}}, \quad \delta F_V = -V_{ws}^2 \int_{R_H}^\infty \frac{dr}{(1 + e^{(r-R_{ws})/a_{ws}})^2}. \quad (7)$$

Using the identity

$$\int_{R_H}^\infty dr \frac{g(r)}{(1 + e^{(r-R_{ws})/a_{ws}})^n} = \Delta^n a_{ws} \int_0^\infty dx \frac{g(a_{ws}x + R_H) e^{-nx}}{(1 + \Delta e^{-x})^n}, \quad \Delta = e^{-(R_H - R_{ws})/a_{ws}},$$

we can neglect δF_H and δF_V in Eq.(5) and (6), assuming $\Delta \ll 1$. Then, F_V in Eq.(6) is independent of k and R_H , and it is enough to minimize the only first term of the most right-hand side of Eq.(5). The integral of the first term is performed with the use of Sommerfeld expansion. In neglecting contributions of relative order $e^{-R_{ws}/a_{ws}}$ [1], it is written as

$$\int_0^\infty dr \frac{g(r)}{1 + e^{(r-R_{ws})/a_{ws}}} = \int_0^{R_{ws}} dr g(r) + \frac{\pi^2 a_{ws}^2}{6} g'(R_{ws}) + \frac{7\pi^4 a_{ws}^4}{360} g'''(R_{ws}) + \dots$$

Since $g'''(r) = 0$ for Eq.(5), we have

$$F_0 = \frac{2}{15} k^2 R_H^5 + k V_{ws} \left(R_H^2 R_{ws} - \frac{1 + b_{ws}}{3} R_{ws}^3 \right), \quad b_{ws} = \left(\frac{\pi a_{ws}}{R_{ws}} \right)^2.$$

It should be noticed that there is no higher-order contribution from the diffuseness parameter. The partial differentials of the above equation with respect to k and R_H yield its minimum value at

$$k = -3 \left(\frac{3}{5} \right)^{3/2} \frac{V_{ws}}{R_{ws}^2 (1 + b_{ws})^{3/2}}, \quad (8)$$

$$R_H^2 = \frac{5}{3} (1 + b_{ws}) R_{ws}^2, \quad V_H(0) = \frac{3}{2} \sqrt{\frac{3}{5}} \frac{V_{ws}}{\sqrt{1 + b_{ws}}}.$$

When employing the values, $V_{ws} = -50$ MeV, $R_{ws} = 5.8$ fm and $a_{ws} = 0.65$ fm in Ref.[1], the above equations provide $\omega = 8.49$ MeV and $V_H(0) = -54.80$ MeV, which reproduce almost the same values obtained by the numerical method mentioned above.

Finally, inserting Eq.(8) into Eq.(3), R_{ho} is described approximately in terms of the WS parameters as

$$R_{ho} \approx B \left(-\frac{R_{ws}^2}{m^* V_{ws}} \right)^{1/4} (1 + b_{ws})^{3/8}, \quad (9)$$

B being a constant. In the above equation, the nucleon mass has been replaced by the effective mass, $M^* = Mm^*$. Eq.(9) well expresses our expectation such that the value of R increases with R_{ws} , and decreases with increasing $(-V_{ws})$ and m^* . Indeed, the first parenthesis of the right-hand side may be derived in the square-well potential with the depth V_{ws} and the width R_{ws} . The diffuseness parameter contributes to the radius positively by $(a_{ws}/R_{ws})^2$.

If the neutron potential, V_n , and effective mass, m_n^* , are different from V_p and m_p^* of the proton, the value of R_n may be different from that of R_p . In the same way, if V_n and m_n^* in the one model are different from those in another model, their R_n 's are different from each other. When comparing the nuclear radius, R_1 in the one framework with R_2 in another one, the following expression is useful,

$$\frac{R_1}{R_2} = \left(\frac{m_2^* V_{ws,2}}{m_1^* V_{ws,1}} \right)^{1/4} \left(\frac{R_{ws,1}}{R_{ws,2}} \right)^{1/2} \left(\frac{1 + b_{ws,1}}{1 + b_{ws,2}} \right)^{3/8}. \quad (10)$$

3 Equations of motion of the mean field models

Eq.(9) and (10) are simple enough to understand the relationship between R_{ho} and the key quantities of the one-body potential. The effective mass and the one-body potential are well-defined quantities in the mean field models. Expecting that such a simple relationship holds approximately in those phenomenological models also, let us investigate how they appear in the equations of motion in the relativistic and non-relativistic models.

In the relativistic nonlinear $\sigma - \omega - \rho$ model, the nuclear Lagrangian is given, using the notations in the literature[14, 16, 22], by

$$\begin{aligned} \mathcal{L} = & \bar{\psi} \left(i\gamma_\mu \partial^\mu - M - g_\sigma \sigma - g_\omega \gamma_\mu \omega^\mu - g_\rho \gamma_\mu \boldsymbol{\tau} \cdot \mathbf{b}^\mu - e\gamma_\mu A^\mu \frac{1 + \tau_3}{2} \right) \psi \\ & + \frac{1}{2} (\partial_\mu \sigma)^2 - \frac{m_\sigma^2}{2} \sigma^2 - \frac{g_3}{3} \sigma^3 - \frac{g_4}{4} \sigma^4 - \frac{1}{4} \omega_{\mu\nu} \omega^{\mu\nu} + \frac{m_\omega^2}{2} \omega_\mu \omega^\mu + \frac{c_4}{4} (\omega_\mu \omega^\mu)^2 \\ & - \frac{1}{4} \mathbf{b}_{\mu\nu} \cdot \mathbf{b}^{\mu\nu} + \frac{m_\rho^2}{2} \mathbf{b}_\mu \cdot \mathbf{b}^\mu + \lambda g_\rho^2 \mathbf{b}_\mu \cdot \mathbf{b}^\mu g_\omega^2 \omega_\nu \omega^\nu - \frac{1}{4} A_{\mu\nu} A^{\mu\nu}. \end{aligned} \quad (11)$$

Then, Euler-Lagrange equation provides us with the equations of motion for the static mean field,

$$(-i\boldsymbol{\alpha} \cdot \boldsymbol{\nabla} + \gamma_0(M + V_\sigma) + V_0)\psi = (E + M)\psi \quad (12)$$

$$(-\nabla^2 + m_\sigma^2) V_\sigma = -g_\sigma^2 \left(\rho_S + \frac{g_3}{g_\sigma^3} V_\sigma^2 + \frac{g_4}{g_\sigma^4} V_\sigma^3 \right), \quad (13)$$

$$(-\nabla^2 + m_\omega^2) V_\omega = g_\omega^2 \left(\rho - \frac{c_4}{g_\omega^4} V_\omega^3 - 2\lambda V_\omega V_\rho^2 \right), \quad (14)$$

$$(-\nabla^2 + m_\rho^2) V_\rho = g_\rho^2 (\rho_p - \rho_n - 2\lambda V_\omega^2 V_\rho), \quad -\nabla^2 V_c = e^2 \rho_p. \quad (15)$$

In the above equations from Eq.(12) to (15), we have defined ψ as a single-particle wave function, and used following notations, $V_\sigma = g_\sigma \sigma$, $V_\omega = g_\omega \omega^0$, $V_\rho = g_\rho b_3^0$ and V_c for the Coulomb potential, $V_c = eA^0$. Moreover, V_0 is given by

$$V_0(\mathbf{r}) = V_\omega(\mathbf{r}) + V_\rho(\mathbf{r})\tau_3 + V_c(\mathbf{r})\frac{1 + \tau_3}{2} \quad (16)$$

with $\tau_3 = +1(-1)$ for protons(neutrons), and the nucleon densities are

$$\rho_S(\mathbf{r}) = \sum_{\alpha \in \tau} \bar{\psi}_\alpha(\mathbf{r})\psi_\alpha(\mathbf{r}), \quad \rho_\tau(\mathbf{r}) = \sum_{\alpha \in \tau} \psi_\alpha^\dagger(\mathbf{r})\psi_\alpha(\mathbf{r}), \quad \rho(\mathbf{r}) = \rho_n(\mathbf{r}) + \rho_p(\mathbf{r}),$$

with $\tau = p$ for protons and $\tau = n$ for neutrons.

Eq.(12) represents the two coupled equations for the upper component, $\psi_u(\mathbf{r})$, and the lower two component, $\psi_d(\mathbf{r})$, of $\psi(\mathbf{r})$. One of them gives

$$\psi_d(\mathbf{r}) = -\frac{1}{2M_\tau^*(\mathbf{r})}i\boldsymbol{\sigma}\cdot\nabla\psi_u(\mathbf{r}), \quad (17)$$

writing the effective nucleon mass, $M_\tau^*(\mathbf{r})$, as

$$M_\tau^*(\mathbf{r}) = \frac{2M + E + V_\sigma(\mathbf{r}) - V_0(\mathbf{r})}{2}. \quad (18)$$

In inserting Eq.(17) into another equation of Eq.(12), we obtain the Schrödinger-like equation as

$$\left(-\nabla\frac{1}{2M_\tau^*(\mathbf{r})}\cdot\nabla + V_\tau(\mathbf{r}) + V_c(\mathbf{r})\frac{1+\tau_3}{2} - i\left(\nabla\frac{1}{2M_\tau^*(\mathbf{r})}\right)\cdot(\nabla\times\boldsymbol{\sigma})\right)\psi_u(\mathbf{r}) = E\psi_u(\mathbf{r}). \quad (19)$$

In the above equation, the nuclear potential, $V_\tau(\mathbf{r})$, is defined by

$$V_\tau(\mathbf{r}) = V_\sigma(\mathbf{r}) + V_\omega(\mathbf{r}) + V_\rho(\mathbf{r})\tau_3. \quad (20)$$

We note that the effective mass, $M_\tau^*(\mathbf{r})$, is written approximately as

$$M_\tau^*(\mathbf{r}) \approx M + \frac{1}{2}\left(V_\sigma(\mathbf{r}) - V_\omega(\mathbf{r}) - V_\rho(\mathbf{r})\tau_3 - V_c(\mathbf{r})\frac{1+\tau_3}{2}\right), \quad (21)$$

using the fact that $2M + E \approx 2M$. For ^{208}Pb , the values of the potentials around the center of the nuclear density are about $V_\sigma \approx -380$ MeV, $V_\omega \approx 306$ MeV and $V_\rho \approx -6$ MeV[22]. It should be noted that the effective mass in the relativistic models is almost isoscalar, and is dominated by V_σ and V_ω in the same way as the spin-orbit potential in the last term of the left-hand side in Eq.(19).

The root-msr's of the point proton and neutron distributions calculated with NL3[22] are listed in Table 1. They are defined as

$$R_\tau^2 = \frac{1}{N_\tau} \sum_{\alpha \in \tau} \int_0^\infty dr r^2 \left(G_\alpha^2(r) + F_\alpha^2(r) \right), \quad (R_\tau)_G^2 = \frac{1}{N_\tau} \sum_{\alpha \in \tau} \int_0^\infty dr r^2 G_\alpha^2(r),$$

$$(R_\tau)_N^2 = \frac{1}{N_\tau} \sum_{\alpha \in \tau} \int_0^\infty dr r^2 \frac{G_\alpha^2(r)}{n_G}, \quad n_G = \int_0^\infty dr G_\alpha^2(r),$$

where $G_\alpha(r)/r$ and $F_\alpha(r)/r$ denote the radial part of the large and the small component of $\psi_\alpha(\mathbf{r})$, respectively, with the normalization, $\int_0^\infty dr (G_\alpha^2(r) + F_\alpha^2(r)) = 1$. Moreover, we have defined $N_\tau = N(Z)$ for $\tau = n(p)$, and n_G for the normalization of the upper component used in $(R_\tau)_N^2$. Table 1 shows also the ratios of $(R_\tau)_G$ and $(R_\tau)_N$ to R_τ in the parentheses. As seen from $(R_\tau)_G$ in Table 1, the contribution of the lower component to R_τ is about 1%, and it is absorbed into $(R_\tau)_N$ which is calculated with the renormalized large component $G_\alpha(r)/\sqrt{n_G}$. Similar results are obtained in other relativistic models. According to these results, we will use the renormalized large component, ignoring the small component, when comparing the relativistic models with the non-relativistic ones below.

We note that in principle, the two-component framework equivalent to the four-component one should be derived by the Foldy-Wouthuysen unitary transformation[9]. Eq.(19) will be used only in the present paper for comparison with non-relativistic models, for simplicity and transparency. In Ref.[4], the calculations of the msr in the relativistic models have been performed within the four-component framework.

	R_n	$(R_n)_G$	$(R_n)_N$	R_p	$(R_p)_G$	$(R_p)_N$
^{48}Ca	3.6050	3.5736(0.991)	3.6082(1.001)	3.3789	3.3522(0.992)	3.3846(1.002)
^{208}Pb	5.7405	5.6888(0.991)	5.7522(1.002)	5.4600	5.4135(0.991)	5.4656(1.001)

Table 1: The root msr of the point neutron(R_n) and proton(R_p) distribution calculated with NL3 for ^{48}Ca and ^{208}Pb . The number is given in units of fm, except for the one in the parenthesis which denotes the ratio to the R_τ . For details, see the text.

In the Skyrme Hartree-Fock approximation in the non-relativistic models, the Schrödinger equation is written as [23, 24],

$$\left(-\nabla \frac{1}{2M_\tau^*(\mathbf{r})} \cdot \nabla + V_\tau(\mathbf{r}) + V_c(\mathbf{r}) \frac{1 + \tau_3}{2} - i\mathbf{W}_\tau(\mathbf{r}) \cdot (\nabla \times \boldsymbol{\sigma}) \right) \varphi(\mathbf{r}) = E\varphi(\mathbf{r}), \quad (22)$$

where using the same notations as in Ref.[24], $M_\tau^*(\mathbf{r})$, $V_\tau(\mathbf{r})$ and $\mathbf{W}_\tau(\mathbf{r})$ are given as,

$$\frac{1}{M_\tau^*(\mathbf{r})} = \frac{1}{M} + \frac{t_1(2 + x_1) + t_2(2 + x_2)}{4} \rho(\mathbf{r}) + \frac{t_2(1 + 2x_2) - t_1(1 + 2x_1)}{4} \rho_\tau(\mathbf{r}), \quad (23)$$

$$\begin{aligned} V_\tau(\mathbf{r}) = & \frac{t_0}{2} \left((2 + x_0)\rho(\mathbf{r}) - (1 + 2x_0)\rho_\tau(\mathbf{r}) \right) + \frac{t_3}{24} (2 + x_3)(2 + \alpha)\rho^{\alpha+1}(\mathbf{r}) \\ & - \frac{t_3}{24} (2x_3 + 1) \left[2\rho^\alpha(\mathbf{r})\rho_\tau(\mathbf{r}) + \alpha\rho^{\alpha-1}(\mathbf{r}) \left(\rho_p^2(\mathbf{r}) + \rho_n^2(\mathbf{r}) \right) \right] \\ & + \frac{t_1(2 + x_1) + t_2(2 + x_2)}{8} K(\mathbf{r}) + \frac{t_2(1 + 2x_2) - t_1(1 + 2x_1)}{8} K_\tau(\mathbf{r}) \\ & + \frac{t_2(2 + x_2) - 3t_1(2 + x_1)}{16} \nabla^2 \rho(\mathbf{r}) + \frac{3t_1(1 + 2x_1) + t_2(1 + 2x_2)}{16} \nabla^2 \rho_\tau(\mathbf{r}) \\ & - \frac{W_0}{2} \nabla \cdot (\mathbf{J}(\mathbf{r}) + \mathbf{J}_\tau(\mathbf{r})), \end{aligned} \quad (24)$$

$$\begin{aligned} \mathbf{W}_\tau(\mathbf{r}) = & \frac{W_0}{2} \nabla (\rho(\mathbf{r}) + \rho_\tau(\mathbf{r})) + \frac{t_1 - t_2}{8} \mathbf{J}_\tau(\mathbf{r}) - \frac{t_1 x_1 + t_2 x_2}{8} \mathbf{J}(\mathbf{r}) \\ \approx & \frac{W_0}{2} \nabla (\rho(\mathbf{r}) + \rho_\tau(\mathbf{r})). \end{aligned} \quad (25)$$

In Eq.(24), $K(\mathbf{r}) = K_n(\mathbf{r}) + K_p(\mathbf{r})$ has been defined with $K_\tau(\mathbf{r}) = \sum_{\alpha \in \tau} |\nabla \varphi_\alpha(\mathbf{r})|^2$, and $\mathbf{J}(\mathbf{r}) = \mathbf{J}_n(\mathbf{r}) + \mathbf{J}_p(\mathbf{r})$, where $\mathbf{J}_\tau(\mathbf{r})$ denotes the spin density given in Ref.[24].

It is seen that Eq.(22) in the non-relativistic models has the same structure as Eq.(19) in the relativistic models. They are composed of the four parts, $M_\tau^*(\mathbf{r})$, $V_\tau(\mathbf{r})$, $V_c(\mathbf{r})$ and the spin-orbit potential. If the strengths and the coordinate-dependences of these parts were the same in the two frameworks, one could not distinguish one framework from another, in spite of their complicated parameter sets. Among the four parts, the last two ones are expected to play a minor role in the present purpose to explore the difference between δR 's in the two frameworks. The Coulomb potential is almost the same, and the strengths of the spin-orbit potentials reproduce experimental values of the single-particle energy levels in both frameworks[14, 25]. In contrast to these, the first two parts are strongly model-dependent. The values of the effective masses are spread out over a wide range [13]. Similarly, there is no reason why the one-body potentials are almost the same in all the mean field models. Hence, the 0.1 fm difference between δR 's may be related to $M_\tau^*(\mathbf{r})$ and $V_\tau(\mathbf{r})$ depending on the different interaction parameters.

This observation is consistent with Eq.(9) and (10) which clearly indicate that the difference problem is related to the effective mass and one-body potential. It is also apparent that they are not independent of each other. On the one hand, the product of the $M_p^*(\mathbf{r})$ and $V_p(\mathbf{r})$

is constrained by hand so as to reproduce the experimental value of R_c in both relativistic and non-relativistic models. On the other hand, there is not a similar constraint on the neutron distribution, but both frameworks predict the values of R_n which are distributed within a narrow range around each average value[4]. If the difference between δR 's is actually related to the effective mass and the one-body potential, there should be another constraint on the variations of these two quantities, which works differently in the relativistic and non-relativistic models.

As one of such candidates, it may be natural to expect the symmetry energy. The symmetry energy coefficient, a_4 , is composed of the potential and kinetic parts[1], which are given in the present relativistic and non-relativistic mean field models, respectively, as[13]

$$a_{4,\text{rel}} = \frac{k_{\text{F}}^2}{6\sqrt{k_{\text{F}}^2 + M_{\sigma}^2}} + \frac{\rho}{2} \frac{g_{\rho}^2}{m_{\rho}^2 + 2\lambda g_{\rho}^2 V_{\omega}^2}, \quad M_{\sigma} = M + V_{\sigma}, \quad (26)$$

$$a_{4,\text{non}} = \left(\frac{3\pi^2}{2}\right)^{2/3} \left(\frac{\rho^{2/3}}{6M} + \frac{-3t_1 x_1 + t_2(5x_2 + 4)}{24} \rho^{5/3}\right) - \frac{2x_0 + 1}{8} t_0 \rho - \frac{2x_3 + 1}{48} t_3 \rho^{\alpha+1}, \quad (27)$$

where k_{F} denotes the Fermi momentum, and ρ the nucleon density in the nuclear matter. Actually, they are related to the difference between the neutron and proton potentials in Eq.(20) and (24), and the effective mass in Eq.(18) and (23). The relationship of a_4 to δR , however, does not seem to be described explicitly. In fact, there is more fundamental restriction on the relationship between the potential and the effective mass. It is known as the Hugenholtz-Van Hove(HVH) theorem[19, 20, 21], which holds in any mean field model for symmetric nuclear matter.

4 Hugenholtz-Van Hove theorem

According to the HVH theorem, the binding energy per nucleon is equal to the Fermi energy in symmetric nuclear matter. Both relativistic and non-relativistic models have been constructed so as to satisfy the theorem at the values of the binding energy of the nucleon to be about -16MeV and of the Fermi momentum to be about 1.3 fm^{-1} . These values are used as inputs in order to fix their free parameters in the nuclear interactions. The Fermi energy is given by the sum of the kinetic and potential energy, so that the strength of the potential and the value of the effective mass are constrained by these inputs. Since the HVH theorem has been proved for the only symmetric nuclear matter[19, 20, 21], however, we will extend the theorem to the relativistic and non-relativistic asymmetric nuclear matter, and utilize the theorem as a guide of the analysis of δR in neutron-rich finite nuclei.

4.1 HVH theorem in the symmetric nuclear matter

Hugenholtz and Van Hove have shown that the following equation holds in the non-relativistic mean field model for symmetric nuclear matter[19, 20, 21],

$$\frac{\varepsilon}{\rho} = E_{\text{F}} \quad \text{for} \quad \frac{d}{d\rho} \frac{\varepsilon}{\rho} = 0, \quad (28)$$

where ε stands for the total energy density of the system, and E_{F} the Fermi energy. The value of ε/ρ represents the binding energy per nucleon, E_{B} , to be written in the non-relativistic models,

as

$$E_B = E_F = \frac{k_F^2}{2m^*M} + V. \quad (29)$$

In the relativistic models, ε/ρ and E_F contain the nucleon mass. Hence, E_B and E_F are given by

$$E_B = \frac{\varepsilon}{\rho} - M = E_F - M.$$

In the present relativistic models, E_F in the symmetric nuclear matter is written as[14]

$$E_F = \sqrt{k_F^2 + M_\sigma^2} + V_\omega, \quad M_\sigma = M + V_\sigma.$$

In setting

$$E_B = K + V, \quad K = \sqrt{k_F^2 + M_\sigma^2} - M_\sigma, \quad V = V_\sigma + V_\omega,$$

K is described as

$$K = \frac{k_F^2}{2M^*}(1 - \delta) \approx \frac{k_F^2}{2M^*}, \quad (30)$$

with $M^* = M + (V_\sigma - V_\omega)/2$ from Eq.(21). We have defined

$$\delta = 1 - \frac{2M^*}{k_F^2} \left(\sqrt{k_F^2 + M_\sigma^2} - M_\sigma \right), \quad (31)$$

and used the fact that $\delta \ll 1$ in taking the values of Ref.[22] for the right-hand side. Thus, in the relativistic models also, E_B is expressed in the form as Eq.(29). Finally, in both relativistic and non-relativistic models, the nuclear potential is inversely proportional to the effective mass, according to the HVH theorem. In the case of Eq.(29), we have

$$V = \frac{a}{m^*} + b, \quad (32)$$

where $a \approx -35$ MeV and $b \approx -16$ MeV for $k_F \approx 1.3$ fm⁻¹ and $E_B \approx -16$ MeV.

Indeed, it is verified that all the relativistic and non-relativistic models employed in the present paper satisfy Eq(28) explicitly. In the non-relativistic models, we have for the protons and neutrons, separately,

$$\frac{\partial \varepsilon}{\partial \rho_\tau} = \frac{k_{F\tau}^2}{2M_\tau^*} + V_\tau = E_{F\tau}, \quad (33)$$

while in the relativistic $\sigma - \omega - \rho$ models,

$$\frac{\partial \varepsilon}{\partial \rho_\tau} = \sqrt{k_{F\tau}^2 + M_\sigma^2} + V_\omega + \tau V_\rho = E_{F\tau}. \quad (34)$$

In the above equations, the total energy density in the non-relativistic models is written as[23, 24]

$$\begin{aligned} \varepsilon = & \frac{K_p}{2M_p^*} + \frac{K_n}{2M_n^*} + \frac{t_0}{4} \left((2 + x_0)\rho^2 - (2x_0 + 1)(\rho_p^2 + \rho_n^2) \right) \\ & + \frac{t_3}{24} \left((2 + x_3)\rho^{\alpha+2} - (2x_3 + 1)\rho^\alpha(\rho_p^2 + \rho_n^2) \right), \end{aligned}$$

where we have defined $K_\tau = 3k_{F\tau}^2\rho_\tau/5$ with $k_{F\tau} = (3\pi^2\rho_\tau)^{1/3}$. In the relativistic models, it is given by

$$\varepsilon = \varepsilon_K + V_\omega\rho + V_\rho(\rho_p - \rho_n) + U_\sigma - U_0,$$

using the abbreviations,

$$\begin{aligned}\varepsilon_K &= \frac{2}{(2\pi)^3} \int_0^{k_{Fp}} d^3k \sqrt{k^2 + M_\sigma^2} + \frac{2}{(2\pi)^3} \int_0^{k_{Fn}} d^3k \sqrt{k^2 + M_\sigma^2}, \\ U_\sigma &= \frac{m_\sigma^2}{2g_\sigma^2} V_\sigma^2 + \frac{g_3}{3g_\sigma^3} V_\sigma^3 + \frac{g_4}{4g_\sigma^4} V_\sigma^4, \quad U_0 = \frac{m_\omega^2}{2g_\omega^2} V_\omega^2 + \frac{c_4}{4g_\omega^4} V_\omega^4 + \frac{m_\rho^2}{2g_\rho^2} V_\rho^2 + \lambda V_\omega^2 V_\rho^2,\end{aligned}\quad (35)$$

which satisfy the equations of motion for the mesons,

$$\begin{aligned}\frac{\partial U_\sigma}{\partial V_\sigma} &= \frac{m_\sigma^2}{g_\sigma^2} V_\sigma + \frac{g_3}{g_\sigma^3} V_\sigma^2 + \frac{g_4}{g_\sigma^4} V_\sigma^3 = -\rho_S, \quad \rho_S = \frac{\partial \varepsilon_K}{\partial M_\sigma}, \\ \frac{\partial U_0}{\partial V_\omega} &= \frac{m_\omega^2}{g_\omega^2} V_\omega + \frac{c_4}{g_\omega^4} V_\omega^3 + 2\lambda V_\omega V_\rho^2 = \rho, \quad \frac{\partial U_0}{\partial V_\rho} = \frac{m_\rho^2}{g_\rho^2} V_\rho + 2\lambda V_\omega^2 V_\rho = \rho_p - \rho_n.\end{aligned}$$

In both relativistic and non-relativistic models, $\partial \varepsilon / \partial \rho_\tau = E_{F\tau}$ holds at any value of ρ or k_F , so that we have for $\rho_p = \rho_n = \rho/2$,

$$\frac{d\varepsilon}{d\rho} = \frac{1}{2} \left(\frac{\partial \varepsilon}{\partial \rho_p} + \frac{\partial \varepsilon}{\partial \rho_n} \right) = \frac{E_{Fn} + E_{Fp}}{2} = E_F, \quad \rho \frac{d\varepsilon}{d\rho} = \frac{d\varepsilon}{d\rho} - \frac{\varepsilon}{\rho} = E_F - \frac{\varepsilon}{\rho},$$

as should be. The last equation yields Eq.(28) for $(d/d\rho)(\varepsilon/\rho) = 0$. Thus, in the mean field models, Eq.(33) and (34), which hold for protons and neutrons separately, are essential for the HVH theorem to be valid.

4.2 HVH theorem in the asymmetric nuclear matter

In order to discuss neutron-rich nuclei using the HVH theorem as a guide, we have to extend the theorem so as to be applicable to the relativistic and non-relativistic asymmetric nuclear matter.

One of the naive ways to the extension may be to minimize the total energy per nucleon, assuming $\rho_n = \nu\rho$ and $\rho_p = (1-\nu)\rho$ for a fixed value of ν [1, 13, 24]. This choice, however, is not appropriate for the present purpose, since E_{Fn} and E_{Fp} remain as in Eq.(33) and (34) without the Coulomb energy. Moreover, if $\rho_n = \nu\rho$ and $\rho_p = (1-\nu)\rho$ were realized in finite nuclei, one would have $\delta R = 0$ even for $N \neq Z$ nuclei. In order to extend the HVH theorem for asymmetric nuclear matter, it is better to avoid these defects.

We require for asymmetric nuclear matter

$$\frac{\partial \varepsilon_{\text{asym}}}{\partial \rho_\tau} = 0, \quad (36)$$

adding $v_c \rho_p$ as the Coulomb term to the total energy density,

$$\varepsilon_{\text{asym}} = \varepsilon + v_c \rho_p, \quad (37)$$

where v_c is a constant. Then, since Eq.(33) and (34) still hold, we have the expression of the binding energy,

$$E_B = E_{F\tau} = \frac{k_{F\tau}^2}{2M_\tau^*} + V_\tau + \frac{1 + \tau_3}{2} v_c, \quad (38)$$

in the non-relativistic models, while in the relativistic models,

$$\begin{aligned}E_B = E_{F\tau} - M &= \sqrt{k_{F\tau}^2 + M_\sigma^2} - M_\sigma + V_\tau + \frac{1 + \tau_3}{2} v_c \\ &= (1 - \delta_\tau) \frac{k_{F\tau}^2}{2M_\tau^*} + V_\tau + \frac{1 + \tau_3}{2} v_c,\end{aligned}\quad (39)$$

where δ_τ is given by Eq.(31) with $k_{F\tau}$ and M_τ^* instead of k_F and M^* , respectively, while V_τ and M_τ^* are given by Eq.(20) and (21) neglecting the Coulomb potential. Eq.(38) and (39) are accepted as the HVH theorem in asymmetric nuclear matter, and imply the relationship between V_τ and m_τ^* as in Eq.(32),

$$V_\tau = \frac{a_\tau}{m_\tau^*} + b_\tau, \quad a_\tau = -(1 - \delta_\tau) \frac{k_{F\tau}^2}{2M}, \quad b_\tau = \begin{cases} E_B, & \tau = n \\ E_B - v_c, & \tau = p, \end{cases} \quad (40)$$

where $\delta_\tau = 0$ in the non-relativistic models, while in the relativistic models, $|\delta_\tau| \ll 1$ being almost constant. The values of $k_{F\tau}^2$, which provide the values of ρ_τ in the relativistic and non-relativistic models, are determined by the two equations in Eq.(36), once v_c is given by hand.

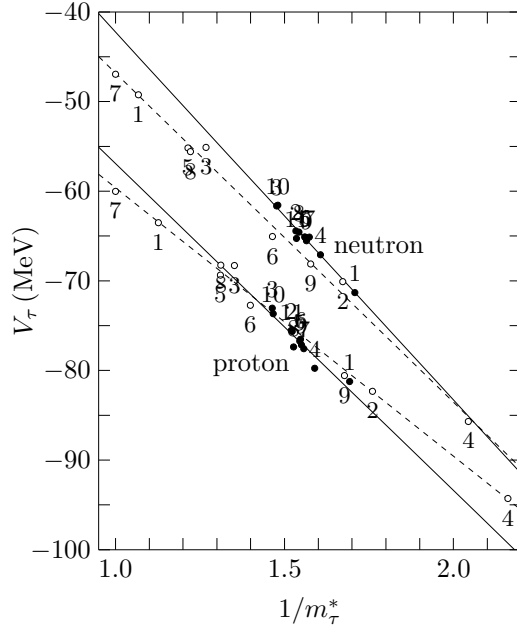


Figure 1: The relationship between the effective mass and the one-body potential for neutrons ($\tau = n$) and protons ($\tau = p$) in the mean field models for asymmetric nuclear matter. The closed circles show the values calculated by the 11 relativistic models, while the open ones show those by the 9 non-relativistic models. Each circles are accompanied by the number which indicates the used model specified in the text. The least square lines are shown for the four groups. The two solid lines are obtained from the closed circles for neutrons and protons, respectively, and the dashed lines from the open circles.

For simplicity, for both relativistic and non-relativistic models, we take v_c from the strength at $r = 0$ of the Coulomb potential for the uniform charge distribution,

$$v_c = \frac{3}{2} \frac{Z\alpha}{r_c A^{1/3}}. \quad (41)$$

It yields $v_c = 22.144$ MeV for ^{208}Pb with $r_c = 1.350$ fm. In employing this value, we obtain Fig.1 for the $1/m_\tau^* - V_\tau$ relationship corresponding to Eq.(40). The closed circles indicate the values from the 11 relativistic models, while the open ones from the 9 non-relativistic models. These models have been employed in Ref.[4]. Each circle is accompanied by the number which shows the used model. The numbering is according to Ref.[4], as 1.L2[15], 2.NLB[15], 3.NLC[15], 4.NL1[26], 5.NL3[22], 6.NL-SH[27], 7.NL-Z[28], 8.NL-S[29], 9.NL3II[30], 10.TM1[31] and 11.FSU[16] for the relativistic nuclear models, and 1.SKI[25], 2.SKII[25], 3.SKIII[32], 4.SKIV[32], 5.SkM*[33], 6.SLy4[24], 7.T6[34], 8.SGII[35] and 9.Ska[36] for the non-relativistic models. The above numbering of the models will be used throughout the present paper.

		a_τ^L	b_τ^L	$\langle a_\tau \rangle$	$\langle b_\tau \rangle$	$\langle m_\tau^* \rangle$	$\langle V_\tau \rangle$	$\langle \rho_\tau \rangle$
Rel	n	-41.059	-1.176	-38.011	-5.918	0.6426	-65.160	0.0832
	p	-36.489	-20.421	-31.530	-28.063	0.6488	-76.742	0.0611
Non	n	-36.743	-10.069	-39.927	-5.840	0.7524	-61.219	0.0903
	p	-29.960	-29.656	-31.168	-27.984	0.7217	-73.256	0.0623

Table 2: The values of the gradient(a_τ^L) and the intercept(b_τ^L) of the least square lines in units of MeV for the relationship between $1/m_\tau^*$ and V_τ in Fig.1. The average values of the coefficients in Eq.(42) are also listed as $\langle a_\tau \rangle$ and $\langle b_\tau \rangle$, together with those of the effective masses, the strengths of the one-body potentials (MeV) and the nuclear matter densities (fm^{-3}) in the relativistic (Rel) and non-relativistic (Non) models. The notations of n and p indicate that the values in the corresponding rows are for neutrons and protons, respectively. For details, see the text.

In Fig.1, the least square lines(LSL) of these circles are drawn by the solid ones for the relativistic models, while by the dashed ones for the non-relativistic models. The LSL's for neutrons and protons are well separated from each other both in the relativistic models and in the non-relativistic ones. The effective mass and the one-body potential are complicated functions of the interaction parameters whose values are different from one another between the mean field models. Nevertheless, as seen in Fig.1, all the circles are almost on their own LSL's.

On the one hand, the circle at $(m_{\tau,i}^*, V_{\tau,i})$ of the model i is given by

$$V_{\tau,i} = a_{\tau,i}/m_{\tau,i}^* + b_{\tau,i}, \quad (42)$$

according to the HVH theorem. On the other hand, LSL satisfies

$$V_{\tau,i}^L = a_\tau^L/m_{\tau,i}^* + b_\tau^L, \quad (43)$$

where a_τ^L and b_τ^L denote the slope and intercept of LSL, respectively. In writing the average value of Eq.(42) as $\langle V_{\tau,i} \rangle$ and that of Eq.(43) as $\langle V_{\tau,i}^L \rangle$, they are equal to each other by the definition of the LSL, $\langle V_{\tau,i} \rangle = \langle V_{\tau,i}^L \rangle$, yielding

$$\langle a_{\tau,i}/m_{\tau,i}^* \rangle + \langle b_{\tau,i} \rangle = a_\tau^L \langle 1/m_{\tau,i}^* \rangle + b_\tau^L. \quad (44)$$

Hence, if the following approximation is valid,

$$\langle a_{\tau,i}/m_{\tau,i}^* \rangle \approx \langle a_{\tau,i} \rangle / \langle m_{\tau,i}^* \rangle, \quad \langle 1/m_{\tau,i}^* \rangle \approx 1 / \langle m_{\tau,i}^* \rangle, \quad (45)$$

then we have

$$\langle m_\tau^* \rangle \langle V_\tau \rangle \approx \langle a_\tau \rangle + \langle b_\tau \rangle \langle m_\tau^* \rangle \approx a_\tau^L + b_\tau^L \langle m_\tau^* \rangle \quad (46)$$

by writing $\langle V_{\tau,i} \rangle = \langle V_\tau \rangle$, $\langle a_{\tau,i} \rangle = \langle a_\tau \rangle$, $\langle b_{\tau,i} \rangle = \langle b_\tau \rangle$ and $\langle m_{\tau,i}^* \rangle = \langle m_\tau^* \rangle$.

In Table 2 are listed the values of the slope a_τ^L and intercept b_τ^L of the LSL. The average values of $a_{\tau,i}$ and $b_{\tau,i}$ calculated by each model are tabulated as $\langle a_\tau \rangle$ and $\langle b_\tau \rangle$. The average values of the effective mass $\langle m_\tau^* \rangle$ and of the strengths of the one-body potentials $\langle V_\tau \rangle$ are also listed, together with the average values of $\rho_{\tau,i}$ as $\langle \rho_\tau \rangle$.

The difference between the values of $\langle a_\tau \rangle$ in the relativistic and non-relativistic models is related to those of $\langle \rho_\tau \rangle$ through the Fermi momentum. The values of $\langle b_\tau \rangle$ are almost the same between the two frameworks, since $\langle b_\tau \rangle$ satisfies the relationship as $\langle E_B \rangle = \langle b_n \rangle$ and $v_c = \langle b_n \rangle - \langle b_p \rangle$, where $\langle E_B \rangle$ denote the average value of $E_{B,i}$, according to Eq.(40).

The values of a_τ^L and b_τ^L depend on the distributions of the points $(m_{\tau,i}^*, V_{\tau,i})$ and have no simple relationship to $\langle \rho_\tau \rangle$, $\langle E_B \rangle$ and v_c . They, however, are implicitly constrained by the HVH

		$\langle m_\tau^* \rangle \langle V_\tau \rangle$	$a_\tau^L + b_\tau^L \langle m_\tau^* \rangle$	$\langle a_\tau \rangle + \langle b_\tau \rangle \langle m_\tau^* \rangle$
Rel	n	-41.872	-41.815	-41.814
	p	-49.790	-49.738	-49.737
Non	n	-46.061	-44.319	-44.321
	p	-52.869	-51.363	-51.364

Table 3: The product of the mean values of the effective mass $\langle m_\tau^* \rangle$ and the one-body potential $\langle V_\tau \rangle$. The numbers are given in units of MeV. For details, see the text.

theorem through Eq.(46). Since the values of v_c and $\langle E_B \rangle$ are almost the same in the relativistic and non-relativistic models, Eq.(46) provides the relationship between the effective mass, the strength of the one-body potential and the nucleon density. This fact implies that the LSL coefficients a_τ^L and b_τ^L are dominated by $\langle \rho_\tau \rangle$ implicitly.

Eq.(46) is rewritten as $a_\tau^L - \langle a_\tau \rangle \approx (\langle b_\tau \rangle - b_\tau^L) \langle m_\tau^* \rangle$, which provides the relationship as $a_\tau^L \gtrsim \langle a_\tau \rangle$ for $b_\tau^L \lesssim \langle b_\tau \rangle$, and $a_\tau^L \lesssim \langle a_\tau \rangle$ for $b_\tau^L \gtrsim \langle b_\tau \rangle$. The non-relativistic models obey the first case, while the relativistic ones the second case. The value of $|b_n^L|$ is made much smaller by the small $\langle m_n^* \rangle$ in the relativistic models, compared with that in the non-relativistic one.

In Table 3, the value of each term in Eq.(46) is listed. It shows that the values of $\langle m_\tau^* \rangle \langle V_\tau \rangle$ are a little larger than those of $\langle a_\tau \rangle + \langle b_\tau \rangle \langle m_\tau^* \rangle$ and $a_\tau^L + b_\tau^L \langle m_\tau^* \rangle$ in the non-relativistic models, because the approximations in Eq.(45) are a little worse in the non-relativistic models than in the relativistic models. This difference, however, is not essential for the present discussions on δR .

In finite nuclei, Eq.(9) indicates that the radius depends on $(-\langle m_\tau^* \rangle \langle V_\tau \rangle)^{-1/4}$. Table 3 implies a possibility that R_n is larger in the relativistic models than in the non-relativistic ones, if the same tendency maintains in finite nuclei. In the mean field models for finite nuclei, however, the effective mass and one-body potential may have complicated coordinate dependences. In order to confirm the above implications for finite nuclei, we need a way to extract from them the values of the effective mass and the strength of the one-body potentials which are appropriate for the use in Eq.(9). Moreover, it is desirable to explore whether or not they are constrained by the HVH theorem as in asymmetric nuclear matter. Although we do not have for finite nuclei an equation like Eq.(36) to yield the HVH constraint in asymmetric nuclear matter, Eq.(46) may be helpful for understanding roles of the HVH theorem in finite nuclei. Bearing these facts in mind, we proceed discussions for finite nuclei from the next section.

5 Simplification of the mean field models

One of the ways to find a common structure of the models is to simplify them without losing their main characteristics. By defining the effective mass and the one-body potential by such a way, we may find their relationships to R and a restriction between them like the HVH lines which are hidden in the complexity of the calculated results of the mean field models for finite nuclei.

In this section, we will analyze the structure of the relativistic and non-relativistic models by simplifying their descriptions as much as possible. As mentioned in §3, R_τ may be a function of $V_\tau(r)$, $M_\tau^*(r)$, $V_c(r)$ and the spin-orbit potential, $V_{\ell s, \tau}(r)$, but among them, it is expected for $V_c(r)$ and $V_{\ell s, \tau}(r)$ to play a minor role in the difference between δR 's in the two frameworks, as $\delta R(V_\tau(r), M_\tau^*(r), V_c(r), V_{\ell s, \tau}(r)) \approx \delta R(V_\tau(r), M_\tau^*(r))$. Using these facts as a guide, let us

express approximately all the Hamiltonians in the both frameworks, using the same basis.

5.1 Nuclear potential and effective mass

The fundamental properties of nuclei are well described with the WS potential[1], and its structure is clear for the present purpose to discuss δR , as in Eq.(10). Hence, we approximate the mean field potential, $V_\tau(r)$, and the effective mass, $M_\tau^*(r)$, in both frameworks by using the WS type function,

$$f_\tau(r) = f_\tau(r, R_\tau, a_\tau) = \frac{1}{1 + \exp((r - R_\tau)/a_\tau)}, \quad (47)$$

that is,

$$V_\tau(r) \approx V_{\text{ws},\tau} f(r, R_{\text{ws},\tau}, a_{\text{ws},\tau}), \quad (48)$$

$$m_\tau^*(r) \approx \begin{cases} 1 + (m_{\text{ws},\tau}^* - 1)f(r, R_{\text{ws},\tau}^*, a_{\text{ws},\tau}^*) - \frac{V_c(r)}{2M} \frac{1 + \tau_3}{2}, & \text{(Rel)}, \\ 1 + (m_{\text{ws},\tau}^* - 1)f(r, R_{\text{ws},\tau}^*, a_{\text{ws},\tau}^*), & \text{(Non)}, \end{cases} \quad (49)$$

where $m_\tau^*(r) = M_\tau^*(r)/M$ is defined, and Rel and Non indicate the relativistic and non-relativistic models, respectively. The three-parameters in the right-hand sides of the above equations are determined by minimizing, for example, for $V_\tau(r)$, the following quantity with respect to $V_{\text{ws},\tau}$, $R_{\text{ws},\tau}$, and $a_{\text{ws},\tau}$,

$$\int_0^\infty dr r^2 \left(V_\tau(r) - V_{\text{ws},\tau} f(r, R_{\text{ws},\tau}, a_{\text{ws},\tau}) \right)^2. \quad (50)$$

Here, the volume integral has been chosen in order to minimize the above deviation, since both $V_\tau(r)$ and $V_{\text{ws},\tau} f(r, R_{\text{ws},\tau}, a_{\text{ws},\tau})$ are expected to have a similar shape to that of the nuclear density whose volume integral value is constrained by the nucleon number. In deriving Eq.(9), we have used $n = 0$ in Eq.(4), since there is not such a constraint on the HO, but since it is important to keep a similarity of the wave functions in the HO and WS.

5.2 Coulomb potential

In the relativistic models, the Coulomb energy is calculated by taking into account the only direct term of the interaction in the same way as for other interactions, while the exchange term is also included in the non-relativistic models. The Coulomb interaction, however, play a minor role in the present purpose on δR , so that we simply express it by that of the uniform charge distribution with the radius, R_{coul} ,

$$V_c(r) \approx V_{\text{sph}}(r), \quad V_{\text{sph}}(r) = \begin{cases} \frac{Z\alpha}{2R_{\text{coul}}} \left(3 - \frac{r^2}{R_{\text{coul}}^2} \right), & r < R_{\text{coul}}, \\ \frac{Z\alpha}{r}, & r > R_{\text{coul}}. \end{cases} \quad (51)$$

The radius R_{coul} is determined by minimizing the deviation:

$$\int_0^\infty dr r^2 \left(V_c(r) - V_{\text{sph}}(r) \right)^2.$$

The value of R_{coul} of the each model will be shown later.

5.3 Spin-orbit potential

We express the spin-orbit potential in the form:

$$V_{\ell s, \tau}(r) = V_{\ell s, \tau} \frac{1}{r} \frac{df_{\tau}(r)}{dr} \boldsymbol{\ell} \cdot \boldsymbol{\sigma}. \quad (52)$$

In the relativistic models, it is written from Eq.(19) as

$$\begin{aligned} V_{\ell s, \tau}(r) &= \frac{1}{r} \frac{d}{dr} \frac{1}{2M_{\tau}^*(r)} \boldsymbol{\ell} \cdot \boldsymbol{\sigma} = -\frac{1}{2M} \frac{1}{m_{\tau}^{*2}(r)} \frac{1}{r} \frac{dm_{\tau}^*(r)}{dr} \boldsymbol{\ell} \cdot \boldsymbol{\sigma} \\ &\approx \frac{1 - m_{\text{ws}, \tau}^*}{2M} \frac{1}{m_{\tau}^{*2}(r)} \frac{1}{r} \frac{d}{dr} f(r, R_{\text{ws}, \tau}^*, a_{\text{ws}, \tau}^*) \boldsymbol{\ell} \cdot \boldsymbol{\sigma}, \end{aligned} \quad (53)$$

neglecting $V_c(r)$ in Eq.(49). In the calculations, the further approximation has been used, as $m_{\tau}^*(r) \approx m_{\tau}^*(R_{\text{ws}, \tau}^*) = (1 + m_{\text{ws}, \tau}^*)/2$.

In the non-relativistic models, the spin-orbit potential of Eq.(25) is approximated as

$$V_{\ell s, \tau}(r) = \frac{W_0}{2r} \frac{d}{dr} (\rho(r) + \rho_{\tau}(r)) \boldsymbol{\ell} \cdot \boldsymbol{\sigma} \approx \frac{W_0 \rho_0}{2} \left(1 + \frac{N_{\tau}}{A}\right) \frac{1}{r} \frac{d}{dr} f(r, R_{\text{den}}, a_{\text{den}}) \boldsymbol{\ell} \cdot \boldsymbol{\sigma}, \quad (54)$$

where the value of W_0 is fixed at 120 MeV fm^5 and we have written the nuclear density as

$$\rho(r) = \rho_p(r) + \rho_n(r) \approx \rho_0 f(r, R_{\text{den}}, a_{\text{den}}),$$

with

$$4\pi\rho_0 \int_0^{\infty} dr r^2 f(r, R_{\text{den}}, a_{\text{den}}) = A.$$

The details of the calculation of the nuclear density will be mentioned in §5.6.

In fact, the spin-orbit potentials are expected not to play an important role in understanding the difference of δR between the relativistic and non-relativistic models, since their strengths are similar and the isospin-dependences are small, in addition to the reason mentioned before.

5.4 A few examples

Before summarizing the results of the present section, let us compare $V_{\tau}(r)$, $\rho_{\tau}(r)$ and $m_{\tau}^*(r)$ from the exact mean field calculations with those of the corresponding simplified Hamiltonian, by taking a few examples. After minimizing Eq.(50), the only values of $V_{\text{ws}, n}$ for the relativistic WS potentials have been multiplied by 0.99, so as to reproduce well the values of R_n in the exact relativistic mean field calculations.

Fig.2 shows the results of the one-body potentials, the effective masses and the neutron and the proton densities for ^{208}Pb calculated with NL3. The solid curves are obtained by the full calculations and the dashed ones by the simplified Hamiltonians. All other relativistic models yield similar results. In non-relativistic models, we show the results for SkM* in Fig.3. These results of SkM* are similar to those of other models except for the effective mass in SLy4. In SLy4, the coordinate dependences of the effective mass are similar to those in Fig.3, but the relation of the magnitude between the $m_{\text{ws}, p}^*$ and $m_{\text{ws}, n}^*$ is opposite to that in other non-relativistic models. It is seen that all the results by simplified versions well reproduce the corresponding ones obtained by the full calculations.

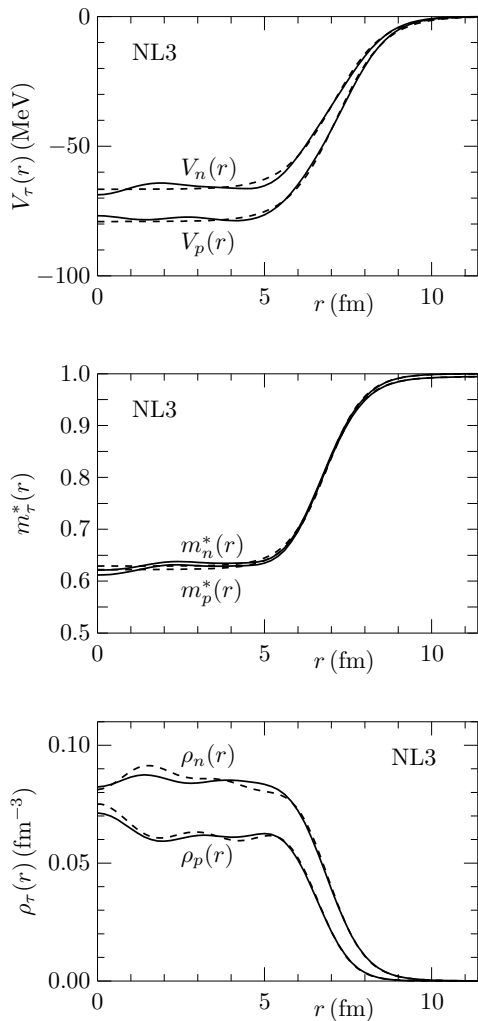


Figure 2: The one-body potentials, the effective masses and the densities for neutrons($\tau = n$) and protons($\tau = p$) in ^{208}Pb . The solid curves are obtained by the relativistic mean field model with NL3, while the dashed ones by its simplified Hamiltonian.

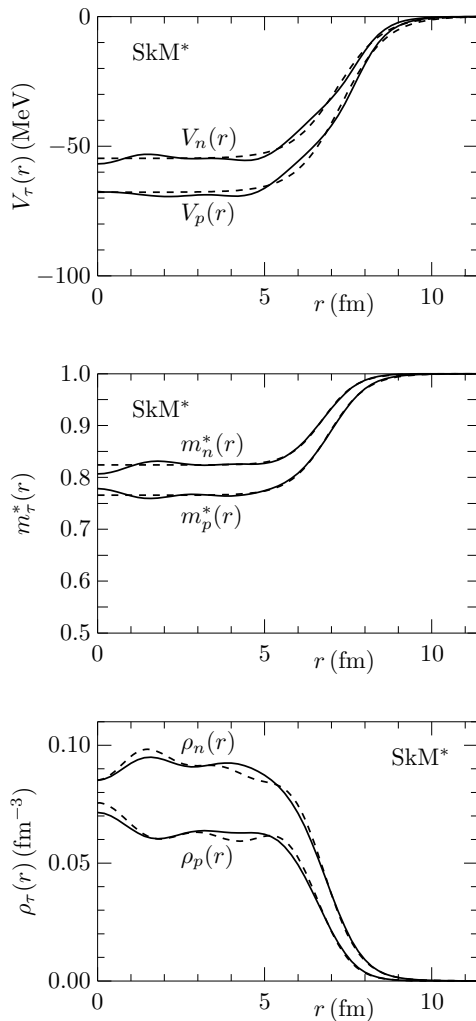


Figure 3: The one-body potentials, the effective masses and the densities for neutrons($\tau = n$) and protons($\tau = p$) in ^{208}Pb . The solid curves are obtained by the non-relativistic mean field model with SkM*, while the dashed ones by its simplified Hamiltonian.

5.5 Results by the simplified models

Table 4 shows the msr's of the point neutron distributions in ^{48}Ca and ^{208}Pb determined in Ref.[4]. Those of the point proton distributions obtained in a similar way are also listed. The errors in the parentheses are given by taking into account the experimental error and the standard deviation of the LSL. Since both relativistic and non-relativistic models employ the experimental values of the msr's of the nuclear charge distributions as an input, the values of R_p in the two frameworks are almost equal to each other, while the values of R_n are larger by about 0.1 fm in the relativistic models than in the non-relativistic ones in both ^{48}Ca and ^{208}Pb . The purpose of the present paper is to understand this difference between R_n 's.

We note that the new data from JLab have been reported in Ref.[5], according to the parity violating electron scattering experiment. It provides δR in ^{208}Pb to be 0.283 ± 0.071 fm. This is almost the same as the value of δR in Table 3 in the relativistic models, and is not incompatible with the non-relativistic one in taking into account their errors. The analysis of the JLab data[5]

		R_n	R_p	δR
^{48}Ca	Rel	3.597(0.021)	3.378(0.005)	0.220(0.026)
	Non	3.492(0.028)	3.372(0.009)	0.121(0.036)
^{208}Pb	Rel	5.728(0.057)	5.454(0.013)	0.275(0.070)
	Non	5.609(0.054)	5.447(0.014)	0.162(0.068)

Table 4: The results of the least square analysis in Ref.[4]. The numbers in the parentheses denote the error which is obtained taking account of the experimental error and the standard deviation of the calculated values from the least square line. All the numbers are given in units of fm. For details, see the text.

is model-dependent as in Ref.[4], and Ref.[37] has obtained $\delta R = 0.19 \pm 0.02$ fm from the JLab data on the basis of the different model-analysis.

Let us summarize the results in the present section for ^{208}Pb . Fig.4 shows the values of $V_{\text{ws},\tau}$ in Eq.(48) for the relativistic and non-relativistic models. The strengths of the neutron potentials are shown by the filled circles, and those of the proton ones by the open circles. It is seen that the non-relativistic ones are distributed over a wide range, as expected, in contrast to those of relativistic models. The straight vertical lines show their average values. The difference between $V_{\text{ws},n} - V_{\text{ws},p}$, however, is almost equal independently of the models, as shown by the crosses and the straight lines indicating their average values. Thus, the difference is only a little larger in the relativistic models than in the non-relativistic ones. This fact implies that the difference between δR 's in the two frameworks may not be due to the symmetry potentials only.

Fig.5 shows the values of $R_{\text{ws},\tau}$ in a similar way as in Fig.4. The closed and open circles for the non-relativistic models are again distributed over a wide region, compared with those of the relativistic ones, although their regions are overlapped. The solid lines express the mean values of the corresponding circles. It is seen that the value of the difference, $\langle R_{\text{ws},p} \rangle - \langle R_{\text{ws},n} \rangle$, in the relativistic models is rather smaller than that in the non-relativistic models as in Table 5. Thus, the spread of the values of $R_{\text{ws},\tau}$ in the non-relativistic models does not seem to cause the difference between δR 's in the two frameworks. The values of R_{coul} are indicated by the crosses for reference.

Fig.6 shows the values of $a_{\text{ws},\tau}$. The straight lines stand for their average values. Those of the relativistic and non-relativistic models are distributed similarly over a wide region, but are small, compared with $R_{\text{ws},\tau}$, as $(a_{\text{ws},\tau}/R_{\text{ws},\tau})^2 \approx 0.01$. The difference between δR 's in the relativistic and non-relativistic models may not be due to these distributions of $a_{\text{ws},\tau}$.

In Fig.7 are shown the values of $m_{\text{ws},\tau}^*$. The closed circles represent those of the neutrons, while the open circles the protons. The straight lines indicate their average values, which are in the relativistic models $\langle m_{\text{ws},n}^* \rangle \approx 0.6321$ and $\langle m_{\text{ws},p}^* \rangle \approx 0.6387$, and in the non-relativistic models $\langle m_{\text{ws},n}^* \rangle \approx 0.7508$ and $\langle m_{\text{ws},p}^* \rangle \approx 0.7207$. As seen in the figure, the circles of the relativistic models are almost at the same value and the ratio, $\langle m_{\text{ws},p}^* \rangle / \langle m_{\text{ws},n}^* \rangle$, is about 1.010, while those of the non-relativistic models are spread out, as in nuclear matter, but the ratio in each model is almost the same and is on average $\langle m_{\text{ws},p}^* \rangle / \langle m_{\text{ws},n}^* \rangle \approx 0.9601$.

Table 5 lists the mean values of the WS parameters, the strengths of the one-body potentials and the effective masses in the present simplified models for the relativistic and non-relativistic mean field ones, respectively. It should be noticed that the values of $\langle m_{\text{ws},\tau}^* \rangle$ and $\langle V_{\text{ws},\tau} \rangle$ are almost the same as those of $\langle m_{\tau}^* \rangle$ and $\langle V_{\tau} \rangle$ in Table 2.

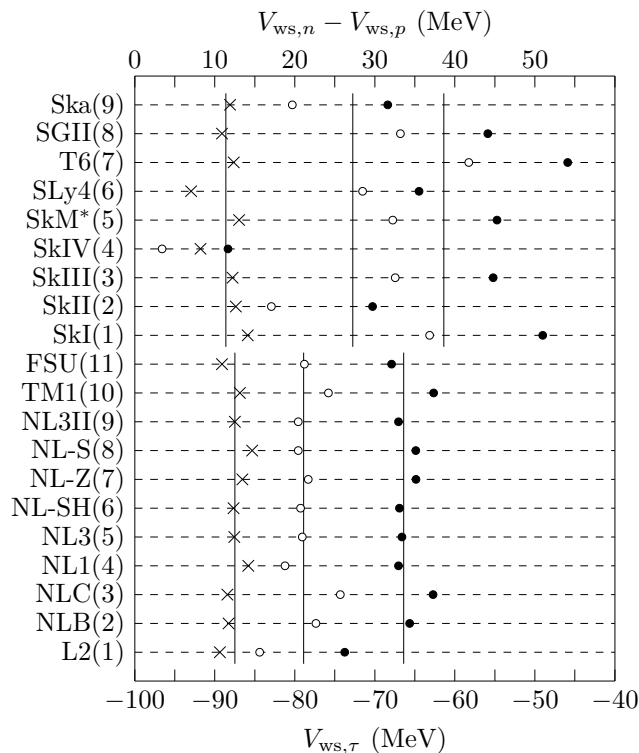


Figure 4: The strength of the one-body potentials for neutrons($\tau = n$) and protons($\tau = p$). On the left-hand side, the relativistic and non-relativistic models are indicated. The closed circles represent the strengths of the neutron potentials, the open ones those of the proton potentials, and the crosses the differences between their two strengths. The vertical lines stand for the average values of the closed and open circles, and of the crosses in the relativistic and non-relativistic models, separately. The scale of the bottom side is for the strength of the potentials, while that of the top side for the difference between the strengths of neutron and proton potentials.

5.6 The proton and neutron distributions

It may be useful to see directly how the difference between δR 's is caused in terms of the neutron and proton densities. We approximate the neutron and proton distributions, $\rho_\tau(r)$, in the mean field models by the Fermi-type function which is widely employed[1, 7]. The approximation is performed for

$$\rho_{ws,\tau}(r) \approx \rho_{0,\tau} f_\tau(r, R_{den,\tau}, a_{den,\tau}), \quad (55)$$

in the same minimization method as in Eq.(50). Since the obtained function satisfies the normalization, $\int d^3r \rho_{ws,\tau}(r) = N_\tau$ with a small error about 0.5%, we slightly correct $R_{den,\tau}$ to satisfy the normalization.

	$\langle R_{ws,n} \rangle$	$\langle R_{ws,p} \rangle$	$\langle a_{ws,n} \rangle$	$\langle a_{ws,p} \rangle$	$\langle V_{ws,n} \rangle$	$\langle V_{ws,p} \rangle$	$\langle m_{ws,n}^* \rangle$	$\langle m_{ws,p}^* \rangle$
Rel	7.046	7.153	0.733	0.719	-66.376	-78.888	0.6321	0.6387
Non	7.096	7.239	0.630	0.632	-61.368	-72.759	0.7508	0.7207

Table 5: The mean values of the Woods-Saxon parameters, the strengths of the one-body potentials and the effective masses in the relativistic and non-relativistic models. The numbers of $\langle R_{ws,\tau} \rangle$ and $\langle a_{ws,\tau} \rangle$ are given in units of fm, and those of $\langle V_{ws,\tau} \rangle$ in units of MeV. For details, see the text.

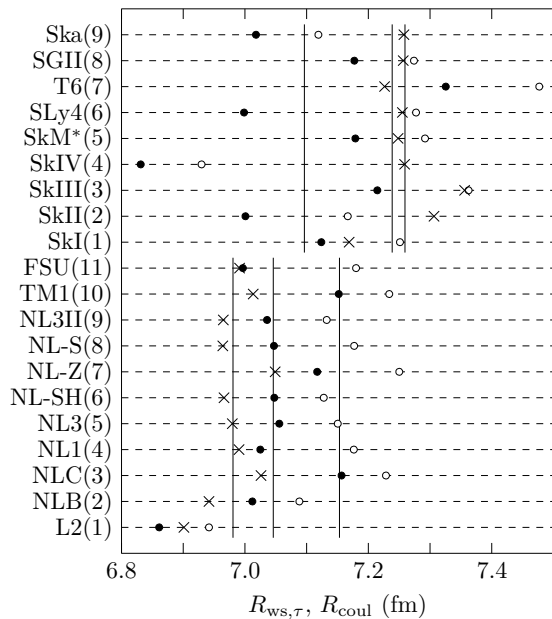


Figure 5: The radius parameters of the Woods-Saxon potentials for neutrons($\tau = n$) and protons($\tau = p$) obtained from the relativistic and non-relativistic mean field models. On the left-hand side, the used relativistic and non-relativistic models are indicated. The closed circles represent the values of the radius parameter $R_{ws,n}$, while the open ones those of $R_{ws,p}$. The crosses stand for the values of the radius parameters of the Coulomb potentials. The vertical lines indicate the average values of the closed and open circles, and of the crosses in the relativistic and non-relativistic models, separately.

The msr, R_τ^2 , by Eq.(55) is given as[1],

$$R_\tau^2 \approx \frac{3}{5} \left(\frac{3N_\tau}{4\pi\rho_{0,\tau}} \right)^{2/3} + \pi^2 a_{den,\tau}^2, \quad (56)$$

which provides the relationship between R_n^2 and R_p^2 as

$$R_n^2 = \frac{R_p^2 - \pi^2 a_{den,p}^2}{(1 - \epsilon)^{2/3}} + \pi^2 a_{den,n}^2, \quad \epsilon = 1 - \frac{Z}{N} \frac{\rho_{0,n}}{\rho_{0,p}}. \quad (57)$$

When keeping order up to $O(\epsilon)$, the difference, $\delta R = R_n - R_p$, is written as

$$\delta R \approx \frac{\epsilon}{3} R_p + \frac{\pi^2}{2} \frac{a_{den,n}^2 - a_{den,p}^2}{R_p}. \quad (58)$$

Table 6 lists the average values of the parameters for the Fermi-type densities in Eq.(55) in the present relativistic and non-relativistic models. Table 7 shows the values of Eq.(56) using the results in Table 6. The average values of R_τ and δR in the mean field models and their simplified versions also are listed in the rows named MF and WS, respectively. It is seen that the values in Eq.(56) and in WS almost reproduce the results of the mean field models.

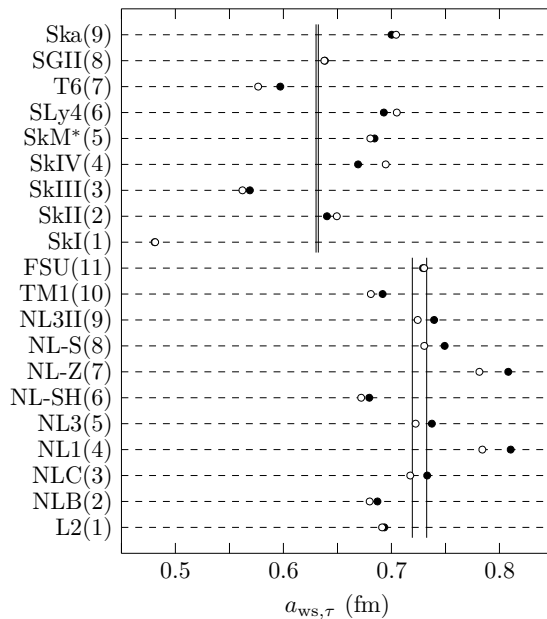


Figure 6: The diffuseness parameters of the Woods-Saxon potentials for neutrons($\tau = n$) and protons($\tau = p$) obtained from the relativistic and non-relativistic mean field models. On the left-hand side, the used relativistic and non-relativistic models are indicated. The closed circles represent the values of the diffuseness parameter $a_{ws,n}$, while the open ones those of $a_{ws,p}$. The vertical lines indicate the average values of the closed and open circles, in the relativistic and non-relativistic models, separately.

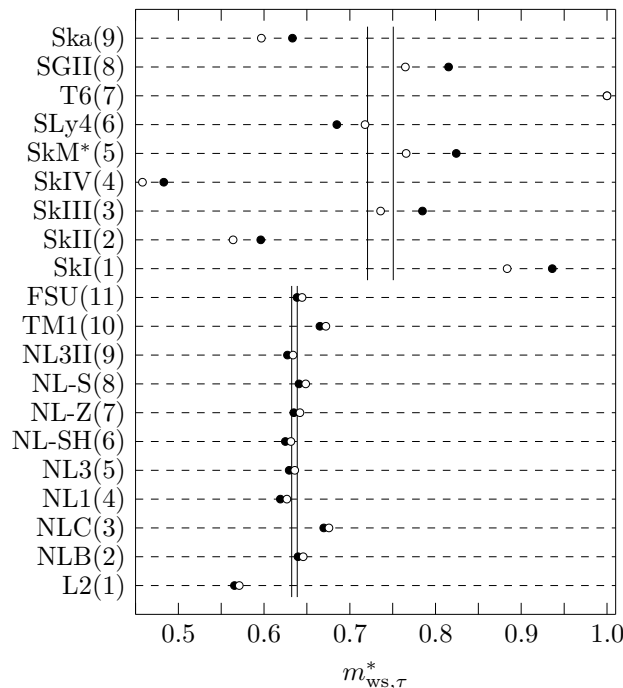


Figure 7: The effective mass of neutrons($\tau = n$) and protons($\tau = p$) obtained from the relativistic and non-relativistic mean field models. On the left-hand side, the used relativistic and non-relativistic models are indicated. The closed circles represent the values of the effective masses of neutrons, while the open ones those of protons. The vertical lines indicate the average values of the closed and open circles, in the relativistic and non-relativistic models, separately.

The values of the two terms in the right-hand side of Eq.(58) are given as

$$\delta R_{\text{rel}} \approx 0.190 + 0.091 = 0.280 \text{ fm}, \quad \delta R_{\text{non}} \approx 0.101 + 0.074 = 0.175 \text{ fm}. \quad (59)$$

Thus the difference about 0.1 fm between δR 's in the relativistic and non-relativistic models mainly comes from the first terms, and the diffuseness parameters yielding the second terms play a rather minor role. It should be noticed that the first term proportional to ϵ disappears, when $\rho_{0,n} = (N/A)\rho$ and $\rho_{0,p} = (Z/A)\rho$.

Since the values of R_p and $\rho_{0,p}$ in the relativistic and non-relativistic models are almost the same, the difference between δR 's in Eq.(58) comes from $\rho_{0,n}$ in ϵ . Table 6 provides

$$\frac{(\rho_{0,n})_{\text{rel}}}{(\rho_{0,n})_{\text{non}}} = 0.944, \quad \frac{(\rho_{0,p})_{\text{rel}}}{(\rho_{0,p})_{\text{non}}} = 0.995.$$

		$\rho_{0,\tau}$	$a_{\text{den},\tau}$	$R_{\text{den},\tau}$	ϵ
Rel	n	0.0860	0.553	6.903	0.1044
	p	0.0625	0.454	6.692	
Non	n	0.0911	0.554	6.766	0.0556
	p	0.0628	0.475	6.672	

Table 6: The mean values of the parameters for the Fermi-type neutron(n) and proton(p) distributions. They are obtained by approximating the densities in the relativistic and non-relativistic mean field models for ^{208}Pb . The values of $\rho_{0,\tau}$ are given in units of fm^{-3} and those of $a_{\text{den},\tau}$ and $R_{\text{den},\tau}$ are in fm. For the definition of ϵ , see the text.

		R_n	R_p	δR
Rel	MF	5.749	5.466	0.283
	WS	5.740	5.457	0.283
	Eq.(56)	5.728	5.451	0.277
Non	MF	5.617	5.455	0.161
	WS	5.621	5.462	0.159
	Eq.(56)	5.629	5.460	0.169

Table 7: The mean values of the root msr's of the neutron(R_n) and proton(R_p) distributions and their difference ($\delta R = R_n - R_p$) obtained by the three approximations for ^{208}Pb . MF indicates the mean values in the relativistic and non-relativistic mean field models, while WS the ones obtained by approximating the mean field potentials by Woods-Saxon potentials. Eq.(56) stands for the equation number in the text used for the calculations of R_τ and δR given in its row. All the values are listed in units of fm. For details, see the text.

The 5.6% decrease of $(\rho_{0,n})_{\text{rel}}$ provides the increase of $(R_n)_{\text{rel}}$ by $0.944^{-1/3} = 1.019$, yielding the 0.1 fm-difference which we are discussing. Fig.2 shows qualitatively such a broadening of the neutron density in NL3, in comparing with that in Fig.3.

In Table 2 are listed the mean values of the neutron and proton densities for the nuclear matter obtained by Eq.(36). Those values are almost the same as the corresponding ones in Table 6. They provide the values of ϵ in Eq.(57) to be 0.1138 and 0.0567 for the relativistic and non-relativistic models, respectively, which are comparable with the values for ^{208}Pb in Table 6. Thus, the various parameters including $\langle m_\tau^* \rangle$ and $\langle V_\tau \rangle$ at $r = 0$ for ^{208}Pb are similar to those for nuclear matter.

It may be noticed that the values listed in the rows of MF in Table 7 are a little different from those of LSA in Table 4, since the former is the mean values of R_τ calculated by the models, while the latter has been obtained by the least squares analysis of the calculated values comparing with the experimental data[4].

6 The HVH lines in ^{208}Pb

We discuss R_τ of the finite nucleus ^{208}Pb on the basis of Eq.(9) and (10). For this purpose, we have to examine if it is appropriate for Eq.(9) and (10) to employ $m_{\text{ws},\tau}^*$ and $V_{\text{ws},\tau}$ defined in Eq.(48) and(49) . When R_τ calculated by the simplified models is expressed in terms of $m_{\text{ws},\tau}^*$ and $V_{\text{ws},\tau}$ as

$$R_\tau \approx B_\tau \left(-\frac{R_{\text{ws},\tau}^2}{m_{\text{ws},\tau}^* V_{\text{ws},\tau}} \right)^{1/4} (1 + b_{\text{ws},\tau})^{3/8}, \quad b_{\text{ws},\tau} = \left(\frac{\pi a_{\text{ws},\tau}}{R_{\text{ws},\tau}} \right)^2, \quad (60)$$

then the value of the coefficient B_τ corresponding to B in Eq.(9) should be almost constant independently of the various interaction parameters of the mean field models. In order to estimate the value of B_τ , both sides except for B_τ of the above equation are calculated for each model, according to §5. The results are listed in the left-hand side named WS in Table 8, where the mean values of B_τ are shown as $\langle B_\tau \rangle$ in units of $(\text{fm}^2 \text{MeV})^{1/4}$ in the relativistic and non-relativistic models, separately. The table shows that the values of the standard deviation(σ) are small enough for our purpose.

The meaning of B_τ may be qualitatively understood according to Ref.[1], where the values of C in Eq.(3) are estimated by summing a single particle radii over the occupied orbits in HO.

		$\langle B_\tau \rangle (\sigma)$	
		WS	MF
Rel	n	5.295 (0.0063)	5.304 (0.0076)
	p	5.243 (0.0151)	5.253 (0.0151)
Non	n	5.288 (0.0217)	5.283 (0.0273)
	p	5.268 (0.0801)	5.261 (0.0685)

Table 8: The mean values of the proportional constant B_τ between the root msr and the function of the Woods Saxon parameters in Eq.(60). The standard deviation σ is given in the parenthesis. WS lists the mean values in using R_τ of the simplified models, while MF shows for reference those in using R_τ of the full mean field approximation. The numbers are written in units of $(\text{fm}^2\text{MeV})^{1/4}$. For details, see the text.

Their approximations yield the values which are in the same order of magnitude as those of B_τ in Table 8, as $B_n \approx 5.44$ for $N = 126$ and $B_p \approx 5.07$ for $Z = 82$ in units of $(\text{fm}^2\text{MeV})^{1/4}$.

We note that the values of σ for protons are larger than those for neutrons in both models. This fact may be due to the Coulomb potential which is not explicitly taken into account in the right-hand side in Eq.(60). If $v_c = 22$ MeV is added to $V_{\text{ws},p}$ by hand for reference, the values of σ for protons become comparable with those for neutrons, as 0.0089 and 0.0217 in the relativistic and non-relativistic models, respectively. We expect, however, that these results do not change the following discussions on the difference between δR 's in the relativistic and non-relativistic models.

It should be also made sure that the 0.1 fm difference between δR 's is not due to the enhancement of $R_{n,\text{rel}}$ by the factor $B_{n,\text{rel}}$. The equation corresponding to Eq.(10) is described as

$$\frac{R_n}{R_p} = \frac{B_n}{B_p} \left(\frac{m_{\text{ws},p}^* V_{\text{ws},p}}{m_{\text{ws},n}^* V_{\text{ws},n}} \right)^{1/4} \left(\frac{R_{\text{ws},n}}{R_{\text{ws},p}} \right)^{1/2} \left(\frac{1 + b_{\text{ws},n}}{1 + b_{\text{ws},p}} \right)^{3/8} \quad (61)$$

Since δR is written as $\delta R = R_p(R_n/R_p - 1)$ and the value of R_p is fixed by the input in both relativistic and non-relativistic models, the difference between δR 's in the two frameworks stems from their values of R_n/R_p . Table 8 provides the ratio of $(\langle B_n \rangle / \langle B_p \rangle)_{\text{rel}} / (\langle B_n \rangle / \langle B_p \rangle)_{\text{non}} = 1.0061$. In the right-hand side of Table 8, the values of $\langle B_\tau \rangle$ in using R_τ from the mean field calculations in Eq.(60) are listed. The table shows that the WS calculations yield almost the same results as those of the mean field ones, as $(\langle B_n \rangle / \langle B_p \rangle)_{\text{rel}} / (\langle B_n \rangle / \langle B_p \rangle)_{\text{non}} = 1.0055$. These values imply that the factor B_τ is not enough to explain the 0.1 fm difference. Thus, it is reasonable to use $V_{\text{ws},\tau}$ and $m_{\text{ws},\tau}^*$ defined in Eq.(48) and (49) in the analysis of δR in ^{208}Pb .

We will show below first how these $V_{\text{ws},\tau}$ and $m_{\text{ws},\tau}^*$ work in Eq.(60) corresponding to Eq.(9), and next how the HVH theorem constrains them.

Provided that Eq.(60) and (61) with the mean values in Table 5 holds, we have for the relativistic and non-relativistic models, respectively, as

$$R_{n,\text{rel}} = (1.0468 \times 1.0047) R_{p,\text{rel}} \approx 5.739 \text{ fm}, \quad (62)$$

$$R_{n,\text{non}} = (1.0329 \times 0.9947) R_{p,\text{non}} \approx 5.612 \text{ fm}. \quad (63)$$

In the parentheses of the right-hand side of the above equations, the first numbers stem from the parenthesis depending on $\langle m_{\text{ws},\tau}^* \rangle$ and $\langle V_{\text{ws},\tau} \rangle$ in Eq.(61), while the second numbers come from the rest of the parentheses. Eq.(62) and (63) show that the difference between R_n and R_p is mainly due to the first numbers in the parentheses, and the second numbers including $\langle R_{\text{ws},\tau} \rangle$

and $\langle a_{ws,\tau} \rangle$ play a minor role in their differences. This fact also implies that the distribution of $R_{ws,\tau}$ and $a_{ws,\tau}$ over a wide region in Fig.5 and 6 is not worrisome for the 0.1 fm problem. The minor role of $a_{ws,\tau}$ is consistent with the results of Eq.(59).

If we put the numbers of R_p obtained by the WS approximation in Table 7 into the right-hand sides of Eq.(62) and(63), then we obtain the values of $R_{n,rel} = 5.739$ fm and $R_{n,non} = 5.612$ fm as in the most right-hand sides. It is seen that they are almost the same values as those in Table 7.

It may be seen more directly that the effective mass and the one-body potentials play an important roles for the difference between δR 's in the two frameworks, by replacing their average values for R_τ in the relativistic models by those in the non-relativistic models. Table 5 and 7 provide

$$R_{\tau,rel} \left(\frac{\langle m_{ws,\tau}^* \rangle \langle V_{ws,\tau} \rangle_{rel}}{\langle m_{ws,\tau}^* \rangle \langle V_{ws,\tau} \rangle_{non}} \right)^{1/4} = \begin{cases} 5.607 \text{ fm}, & \tau = n, \\ 5.403 \text{ fm}, & \tau = p, \end{cases} \quad (64)$$

The above values are smaller than those of R_τ for the non-relativistic models in Table 7, showing essential roles of $\langle m_{ws,\tau}^* \rangle \langle V_{ws,\tau} \rangle$ in R_τ . The above equations yield $\delta R = 0.204$ fm, which should be compared with $\delta R = 0.159$ fm in WS for the non-relativistic models in Table 7. The difference between δR 's in the two frameworks reduces from 0.124 fm to 0.045 fm by 64%.

Now, let us discuss the constraint on $m_{ws,\tau}^*$ and $V_{ws,\tau}$ due to the HVH theorem. In Eq.(62) to (64), we have assumed the relationship between the average values of $m_{ws,\tau}^*$ and $V_{ws,\tau}$ in order to emphasize their roles in the 0.1 fm problem. The more detailed analysis using the values of $m_{ws,\tau}^*$ and $V_{ws,\tau}$ from each model will be made below.

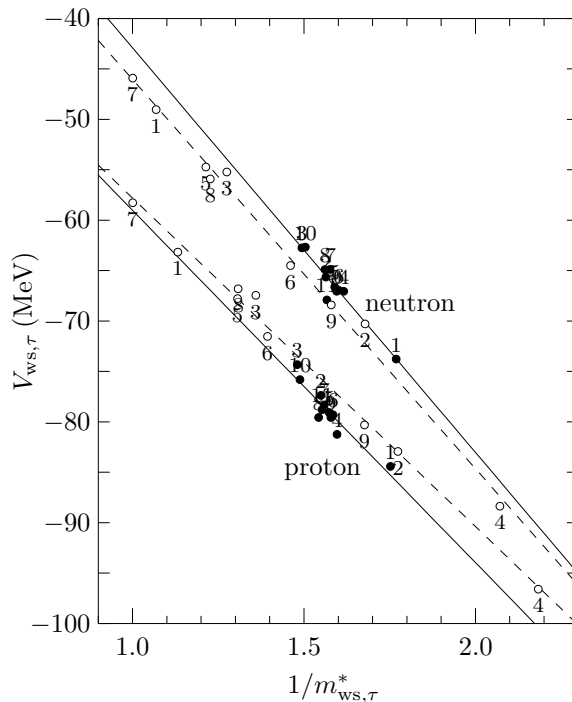


Figure 8: The relationship between the effective mass and the one-body potential for neutrons($\tau = n$) and protons ($\tau = p$) in the mean field models for ^{208}Pb . The closed circles show the values calculated by the 11 relativistic models, while the open ones show those by the 9 non-relativistic models. The least square lines are shown for the four groups. The two solid lines are obtained from the closed circles for neutrons and protons, respectively, and the dashed lines from the open circles.

	Rel			Non		
	$a_{ws,\tau}^L$	$b_{ws,\tau}^L$	r	$a_{ws,\tau}^L$	$b_{ws,\tau}^L$	r
n	-40.120	-2.795	0.958	-38.609	-7.438	0.997
p	-34.933	-24.098	0.937	-32.588	-25.215	0.997

Table 9: The values of the gradient($a_{ws,\tau}^L$) and the intercept($b_{ws,\tau}^L$) of the least square line for the relationship between the depth of the one-body potential and the nucleon effective mass in Fig.8. The numbers of $a_{ws,\tau}^L$ and $b_{ws,\tau}^L$ are given in units of MeV. The values of the correlation coefficient, r , are also listed. For details, see the text.

In Fig.8 are plotted the values of $V_{ws,\tau}$ in Fig.4 and those of $m_{ws,\tau}^*$ in Fig.7 in the $1/m_{ws,\tau}^* - V_{ws,\tau}$ plane. The closed circles show the values for neutrons and protons in the relativistic models, while the open circles in the non-relativistic models. The numbers attached to each circle indicate the used model, according to the numbering mentioned in §4.2. The pair of the same number represent the values for neutrons and protons calculated by the same model.

The slanting lines are obtained by the least square method for the values of each group. The upper and lower solid lines are drawn for neutrons and protons in the relativistic models, respectively, while the upper and lower dashed lines are in the non-relativistic models. It is remarkable that the values of each group well follow the corresponding line, and that the four lines are well separated from one another, as in Fig.1 for nuclear matter. We notice that the only FSU(11)[16] among the relativistic models yields a point on the neutron line for the non-relativistic models. This may reflect the fact that FSU has added two additional parameters to the Lagrangian of, for example, NL3(5)[22], so as to reduce the value of R_n . The values of the gradient($a_{ws,\tau}^L$) and the intercept($b_{ws,\tau}^L$) of the LSL,

$$V_{ws,\tau} = a_{ws,\tau}^L/m_{ws,\tau}^* + b_{ws,\tau}^L, \quad (65)$$

are listed in Table 9 for relativistic(Rel) and non-relativistic(Non) models. The values of the correlation coefficient, r , are also shown, which are nearly equal to 1.

In Fig.8, it is seen that the variation of the effective mass and the strength of the one-body potential in finite nuclei is also constrained in a similar way to that in Fig.1 for nuclear matter. In order to see if the similarity is due to the HVH theorem, we compare the coefficients of the LSL for ^{208}Pb in Table 9 with those of Eq.(43) for nuclear matter listed in Table 2. The coefficients of Eq.(43) have shown to be constrained by the HVH theorem through Eq.(46). It is seen in Table 2 and 9 that the values of the corresponding coefficients are not the same as each other, but the magnitude relation of the corresponding two values are almost the same as those of other pair. More important values for the present discussion is those in Eq.(46). In Table 10 is listed one of the values in Eq.(46), $\langle a_\tau \rangle + \langle b_\tau \rangle \langle m_\tau^* \rangle$, in the first column, and the corresponding values obtained from Table 5 and 9 in the second and the last column. It is seen that the values for nuclear matter in the first column are almost the same as those for ^{208}Pb in other columns. Since the values in the first column is nothing but the results due to the HVH theorem, it is concluded that those in the second and third columns also reflect the constraint by the theorem.

The HVH theorem constrains variances between $\langle m_\tau^* \rangle$, $\langle V_\tau \rangle$ and $\langle \rho_\tau \rangle$ in the same way for the relativistic and non-relativistic models as in Eq.(46). If one of their values is different between the two frameworks, others also may be different between them. The HVH theorem seems to be inherent in the mean field approximation for finite nuclei also. From now on, we will refer to the LSL as the HVH line.

		$\langle a_\tau \rangle + \langle b_\tau \rangle \langle m_\tau^* \rangle$	$\langle m_{ws,\tau}^* \rangle \langle V_{ws,\tau} \rangle$	$a_{ws,\tau}^L + b_{ws,\tau}^L \langle m_{ws,\tau}^* \rangle$
Rel	n	-41.814	-41.956	-41.887
	p	-49.737	-50.386	-50.324
Non	n	-44.321	-46.075	-44.193
	p	-51.364	-52.437	-50.760

Table 10: The values for the combination composed of the effective mass and the coefficients of the least square line for asymmetric nuclear matter(the first column) and for ^{208}Pb (the third column) in the relativistic and non-relativistic models. The values of the product of the effective mass and the strength of the one-body potential is also listed in the second column for ^{208}Pb . All the numbers are given in units of MeV. For details, see the text.

	$V_{ws,\tau}^{\text{rel}}(\langle m_\tau^* \rangle_{\text{rel}})$	$V_{ws,\tau}^{\text{non}}(\langle m_\tau^* \rangle_{\text{rel}})$	$V_{ws,\tau}^{\text{non}}(\langle m_\tau^* \rangle_{\text{non}})$
n	-66.264	-68.517	-58.865
p	-78.792	-76.238	-70.434
$V_n - V_p$	12.528	7.721	11.569

Table 11: The neutron(n) and proton(p) potentials at the mean value of the effective mass. The numbers are given in units of MeV. For details, see the text.

We explore in more detailed roles of $m_{ws,\tau}^*$ and $V_{ws,\tau}$ in Eq.(64) separately, by using the HVH lines in Fig.8. Fig.9 is obtained by enlarging Fig.8 around $1/m_{ws,\tau}^* \approx 1.3 \sim 1.7$. The four vertical lines are added indicating the values of $1/\langle m_{ws,\tau}^* \rangle$, $\langle m_{ws,\tau}^* \rangle$ being the mean value of the effective mass in Table 5. We notice, on the one hand, that the distance between two solid lines for the relativistic models is about 12.5 MeV at a fixed value of $1/m_{ws,\tau}^*$, as listed in Table 11. It is almost the same as the mean value of $V_3 = V_{ws,n} - V_{ws,p}$ in Fig.4. This is because of $m_{ws,n}^* \approx m_{ws,p}^*$ in the relativistic models. On the other hand, in the non-relativistic models, the distance between the two dashed lines for the same value of $1/m_{ws,\tau}^*$ is about 7.7 MeV, in spite of the fact that $V_3 \approx 11.6$ MeV as in Table 11. This is because, in the non-relativistic models, the value of the neutron effective mass is larger than that of the proton one, except for SLy4(6)[24], as in Fig.7. The value of $V_3 \approx 11.6$ MeV is approximately kept by providing neutrons and protons with different effective masses. As seen below, it is essential for understanding 0.1 fm difference that the values of the effective mass for neutrons are different from the ones for protons in the non-relativistic models, while those in the relativistic models are almost the same.

In Fig.9, we have specified the six points on the HVH lines, where X_n , Y_n and Z_n are on the neutron lines and others on the proton lines. X_n and Y_n are the cross point of the $1/\langle m_{ws,n}^* \rangle_{\text{rel}}$ line and the HVH lines for the neutrons in the relativistic and non-relativistic models, respectively, while Z_n that of the $1/\langle m_{ws,n}^* \rangle_{\text{non}}$ line and the HVH line in the non-relativistic models. The other three points, X_p , Y_p and Z_p are plotted in similar ways.

First, we compare the value of R_n at the point $X_n(R_{n,\text{rel}})$ with that at point $Z_n(R'_{n,\text{non}})$, through the point Y_n . From this bypath, it is seen how a role of the effective masses is different from that of the potential. In taking account of $m_{ws,\tau}^*$ - and $V_{ws,\tau}$ -dependences only, Eq.(60)

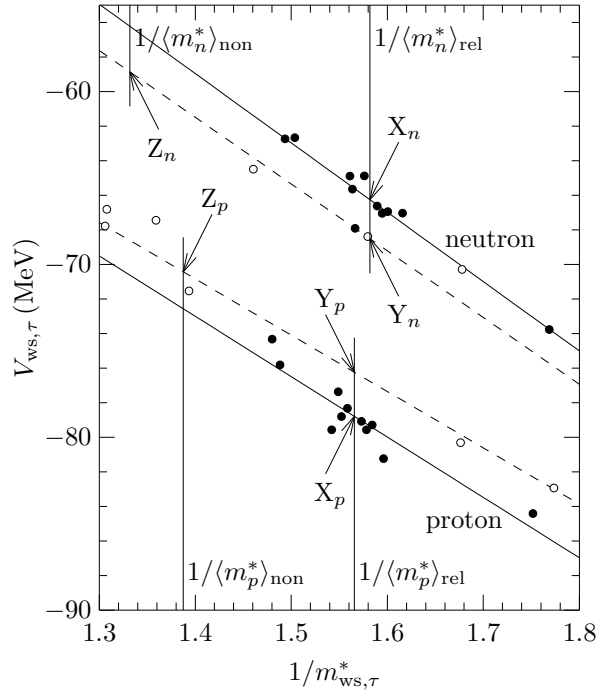


Figure 9: The relationship between the effective mass and the one-body potential for neutrons ($\tau = n$) and protons ($\tau = p$) in the mean field models for ^{208}Pb . This is obtained by enlarging Fig.8 around $1/m_{\text{ws},\tau}^* = 1.5$. The vertical lines show the values of $1/\langle m_{\text{ws},\tau}^* \rangle$, $\langle m_{\text{ws},\tau}^* \rangle$ being the average value of $m_{\text{ws},\tau}^*$ in the relativistic and non-relativistic model. The cross points of the vertical lines with the least square lines for neutrons are indicated as X_n , Y_n and Z_n , and those for protons as X_p , Y_p and Z_p . For details, see the text.

provides the relationship

$$R_{n,\text{int}} = \left(\frac{a_{\text{ws},n,\text{rel}}^{\text{L}} + \langle m_{\text{ws},n}^* \rangle_{\text{rel}} b_{\text{ws},n,\text{rel}}^{\text{L}}}{a_{\text{ws},n,\text{non}}^{\text{L}} + \langle m_{\text{ws},n}^* \rangle_{\text{rel}} b_{\text{ws},n,\text{non}}^{\text{L}}} \right)^{1/4} R_{n,\text{rel}}, \quad (66)$$

$$R'_{n,\text{non}} = \left(\frac{a_{\text{ws},n,\text{non}}^{\text{L}} + \langle m_{\text{ws},n}^* \rangle_{\text{rel}} b_{\text{ws},n,\text{non}}^{\text{L}}}{a_{\text{ws},n,\text{non}}^{\text{L}} + \langle m_{\text{ws},n}^* \rangle_{\text{non}} b_{\text{ws},n,\text{non}}^{\text{L}}} \right)^{1/4} R_{n,\text{int}}, \quad (67)$$

where $R_{n,\text{int}}$ denotes R_n at the point Y_n . By inserting the values in Table 5 and 9 into the above equations, and assuming $R_{n,\text{rel}}$ to be equal to the mean value in Table 7, we obtain

$$R_{n,\text{int}} = 5.692 \text{ fm}, \quad R'_{n,\text{non}} = 5.664 \text{ fm}. \quad (68)$$

Throughout these paths, the values of $\langle R_{\text{ws},n} \rangle$ and $\langle a_{\text{ws},n} \rangle$ of the relativistic models are not changed. Hence, from X_n to Y_n , $V_{\text{ws},n}$ only is changed and becomes deeper, so that the value of R_n is decreased from 5.740 fm in Table 7 to 5.692 fm. From Y_n to Z_n , the potential becomes shallower, but the value of the effective mass is increased and a role of the kinetic part as a repulsive force declines. As a result, the value of R_n further shrinks from 5.692 fm to 5.664 fm, as in Eq.(68). The final value $R'_{n,\text{non}} = 5.664$ fm should be compared with the mean value of $R_{n,\text{non}} = 5.621$ fm in the non-relativistic models in Table 7. The difference between these two values is 0.043 fm, while Table 7 shows 0.119 fm for the difference between the mean values, $R_{n,\text{rel}} - R_{n,\text{non}}$. Thus, the value of R_n in the relativistic models approaches to that in the non-relativistic models, following the path under the constraint of the HVH theorem on $V_{\text{ws},\tau}$ and $m_{\text{ws},\tau}^*$.

Next, R_p is analyzed in a similar way. Assuming $R_{p,\text{rel}}$ at X_p is equal to the mean value of $R_{p,\text{rel}}$ in WS of Table 7, its value increases from 5.457 fm to $R_{p,\text{int}} = 5.502$ fm, following the path from X_p to Y_p , as the strength of $|V_{\text{ws},p}|$ decreases. From Y_p to Z_p , the value of R_p decreases from $R_{p,\text{int}} = 5.502$ fm to $R'_{p,\text{non}} = 5.445$ fm, in the same way as that of R_n from Y_n to Z_n . The final value of $R'_{p,\text{non}}$ returns to the almost original value of $R_{p,\text{rel}}$ at X_p , since both values of R_p at X_p for the relativistic models and at Z_p for the non-relativistic models are fixed according to the experimental value of R_c as an input in these mean field models.

In the above analysis, it should be noticed that the value of $\langle m_{\text{ws},n}^* \rangle_{\text{non}}$ is larger than that of $\langle m_{\text{ws},p}^* \rangle_{\text{non}}$ as in Table 5. Owing to the fact, the path from Y_n to Z_n is longer than that from Y_p to Z_p as seen in Fig.9. This difference also works to make R_n smaller in the path from Y_n to Z_n .

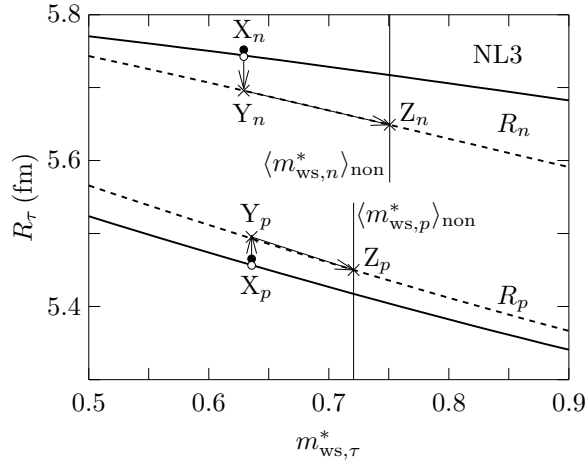


Figure 10: The root msr as a function of the effective mass for $\tau = n$ and $\tau = p$ in NL3. The closed circle is obtained by the full mean field approach, and the open one by the simplified Hamiltonian of NL3. The solid curves are obtained by using the least square lines in the relativistic models in Fig.9, while the dashed ones by using those in the non-relativistic models for the relationship between $m_{\text{ws},\tau}^*$ and $V_{\text{ws},\tau}$. In these curves, the values of the Woods-Saxon parameters, $R_{\text{ws},\tau}$ and $a_{\text{ws},\tau}$, are taken from those determined by NL3. The vertical lines indicate the average values of the effective masses in the non-relativistic models. The points, X_n , Y_n etc., are defined in the same way as in Fig.9, except for X_n and X_p which stand for the open circles. For details, see the text.

In Fig.10 is shown the change of R_τ by the above two steps in the case of NL3(5) as an example. The closed and open circles indicate the values of R_τ in the full mean field calculation and in the simplified one in §5, respectively, at the value of $m_{\text{ws},\tau}^*$ for NL3. The solid lines show R_τ as a function of $m_{\text{ws},\tau}^*$ which are calculated by keeping the values of $R_{\text{ws},\tau}$ and $a_{\text{ws},\tau}$ of NL3 and using $V_{\text{ws},\tau}$ given by the HVH line for the relativistic models in Fig.8. The closed and open circles are seen to be almost on the lines. The dashed lines also show R_τ , but using $V_{\text{ws},\tau}$ given by the HVH line for the non-relativistic models in Fig.8. The points, X_τ , Y_τ and Z_τ correspond to those in Fig.9, but X_τ is the place where NL3 provides $m_{\text{ws},\tau}^*$, instead of $\langle m_{\text{ws},\tau}^* \rangle$. It is seen that the value of R_n decreases by the first step from X_n to Y_n , and also by the second steps from Y_n to Z_n , while the one of R_p returns to the almost original value at X_p by the second step from Y_p to Z_p . The change of R_τ from X_τ to Y_τ is due to the change of the depth of the one-body potential. The decrease of R_τ from Y_τ to Z_τ with the increasing $m_{\text{ws},\tau}^*$ is understood

by Eq.(60) and(65) which yield

$$m_{ws,\tau}^* = -\frac{1}{b_{ws,\tau}^L} \left(a_{ws,\tau}^L + \frac{B_\tau^4}{R_\tau^4} R_{ws,\tau}^2 (1 + b_{ws,\tau})^{3/2} \right). \quad (69)$$

The simultaneous equations of Eq.(60) and (65) as unknowns variables $\langle m_{ws,\tau}^* \rangle$ and $\langle V_{ws,\tau} \rangle$ also reproduce well the values of Table 5.

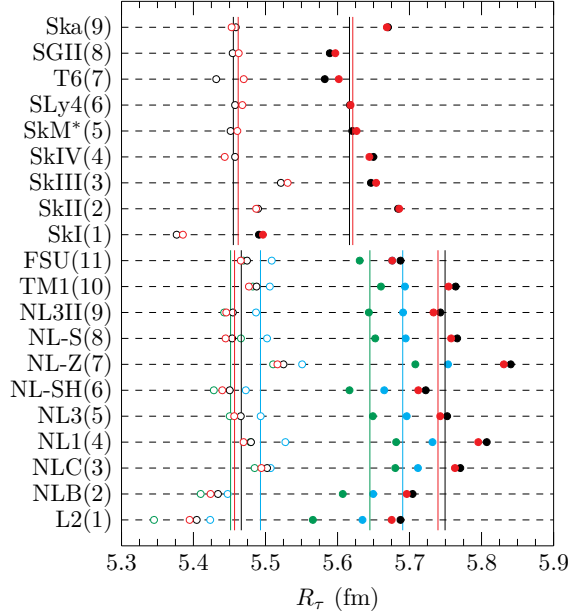


Figure 11: The root msr R_τ of ^{208}Pb calculated in the relativistic and non-relativistic models. On the left-hand side, the used models are indicated. The black closed and open circles are obtained by the full mean field approximations for the neutrons($\tau = n$) and protons($\tau = p$), respectively. The red ones are by the simplified Hamiltonian for each model. The blue ones are obtained through the first step discussed in the text, while the green ones by the second step. The vertical lines show the average values of the same color circles, respectively. For details, see the text.

Fig.11 shows the values of R_τ which are obtained by the same procedure as in Fig 10 for all the relativistic mean field models taken in the present paper. The black and red circles show the results of the full mean field calculations and the simplified ones in §5, respectively, where the closed circles are for neutrons and the open circles for protons. The vertical lines indicate their mean values. It is seen that the simplified calculations well reproduce the values of R_τ by the full calculations. Those for the non-relativistic models also are shown in the same way.

The blue circles are obtained by the first step mentioned in Fig.10, while the green ones by the second step. All the models show the similar change of R_τ as in Fig.10 such that the values of R_n decrease by the two steps, while those of R_p come back to almost the same values by the second step.

Fig.12 shows the values of δR , using the same designating symbols as in Fig.11. The values

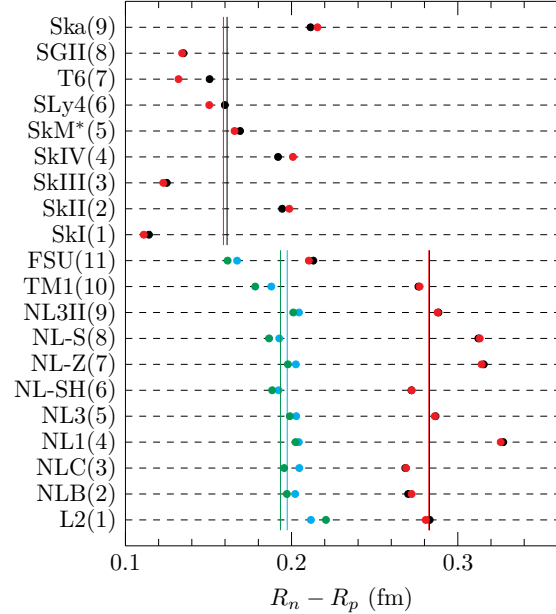


Figure 12: The difference between the root msr's of the neutron and the proton distribution in ^{208}Pb calculated in the relativistic and non-relativistic models. On the left-hand side, the used models are indicated. The black closed circles are obtained by the full mean field approximations, and the red ones by the simplified Hamiltonian for each model. The blue ones are obtained through the first step, while the green ones through the second step discussed in the text. The vertical lines show the average values of the same color circles, respectively. For details, see the text.

	Rel			Non
	Red	Blue	Green	Red
R_n	5.740	5.691	5.645	5.621
R_p	5.457	5.493	5.452	5.462
δR	0.283	0.197	0.193	0.159

Table 12: The average values of the root msr of the proton and neutron distributions in the relativistic(Rel) and non-relativistic(Non) models in various approximations. Red, Green and Blue indicate the average values corresponding to those in Fig.11 and 12, respectively. All the numbers are given in units of fm. For details, see the text.

from the two steps shown by the green circles are almost the same as the blue ones obtained by the first step, since the values of R_p return to the original ones by the second step.

The results of R_τ and δR in Fig.11 and 12 are summarized in Table 12 in units of fm. The mean values of R_τ in the relativistic models are listed in the columns named Red, Blue and Green according to the colors of those figures. From Red to Green, the value of R_n decreases, while that of R_p increases from Red to Blue and decreases from Blue to Green, up to almost the Red one, as shown in the figures. In changing the values V_τ and m_τ^* in the relativistic models following the HVH lines, the value of δR shrinks from 0.283 fm to 0.193 fm, which should be compared with 0.159 fm of the non-relativistic models. The difference between δR 's in the relativistic and non-relativistic models becomes smaller by 73%, changing its value from 0.124 fm to 0.034 fm.

It is concluded that most of the 0.1 fm difference between δR 's in the relativistic and non-relativistic models is attributed to the difference between the values of their V_τ and m_τ^* , which are constrained by $\rho_{0,\tau}$ through the HVH theorem. The remaining difference may be caused by the sum of many small contributions, in addition to those from $R_{ws,\tau}$, $a_{ws,\tau}$ and B_τ , from the used approximations. The exchange term of the Coulomb force, the center of mass correction, the small component of the wave functions, etc., are also managed differently in the two frameworks. Discussions on those effects, however, are beyond the present purpose.

7 Summary

Ref.[4] has pointed out that the neutron skin thickness defined by $\delta R = R_n - R_p$ in ^{208}Pb is larger by about 0.1 fm in the relativistic mean field models than in the non-relativistic ones. Here, R_n and R_p represent the root msr of the point neutron and proton distributions in the nucleus, respectively. The value of the charge radius R_c of ^{208}Pb is about 5.503 fm. The 0.1 fm difference is not small for nuclear physics[1, 10, 17, 18], but also for astrophysics[3, 5, 18]. In this paper, it has been investigated why the difference is avoidable in the present mean field models, even though both relativistic and non-relativistic models are constructed phenomenologically with free parameters to be fixed by experimental values.

The value of R_p is one of the most important inputs, together with the binding energy per nucleon and the Fermi momentum in nuclear matter in all of the phenomenological models[14, 24]. The relationship between R_p and R_c is unambiguously defined theoretically[8], and the latter is observed experimentally through electromagnetic probes, whose reaction mechanism are well understood[6, 7, 9]. Hence, the 0.1 fm problem is due to the difference between the values of R_n in the two frameworks.

It is shown that the values of R_τ are dominated by those of $(-m_\tau^*V_\tau)^{-1/4}$, where m_τ^* and V_τ represent the effective mass in units of M and the strength of the one-body potential near the center of the nucleus, respectively, and the subscript indicates $\tau = p$ for protons and $\tau = n$ for neutrons. Although m_τ^* and V_τ are complicated functions of the interaction parameters in the phenomenological models, they are not independent of each other. Their variations are constrained together with the nucleon density ρ_τ by the Hugenholtz-Van Hove(HVH) theorem[19, 20, 21].

In writing the average values of m_τ^* and V_τ in each framework as $\langle m_\tau^* \rangle$ and $\langle V_\tau \rangle$, respectively, their product is approximately expressed by the HVH equation as $\langle m_\tau^* \rangle \langle V_\tau \rangle \approx a_\tau + b_\tau \langle m_\tau^* \rangle$, where a_τ and b_τ are constants. The values of a_τ and b_τ depend on the average values of ρ_τ , the binding energy per nucleon E_B and Coulomb energy v_c of the corresponding asymmetric nuclear matter with N and Z . Since the values of E_B and v_c are almost the same in the relativistic and non-relativistic models, the difference between the two frameworks in the right-hand side of the HVH equation is attributed to the difference between the values of $\langle \rho_\tau \rangle$ and $\langle m_\tau^* \rangle$. Indeed, the values of $\langle \rho_\tau \rangle$ and $\langle m_\tau^* \rangle$ in the nuclear matter in Table 2 are almost the same as those for ^{208}Pb in Table 5 and 6. The difference of the right-hand side of the HVH equation for the two frameworks is expressed by $\langle m_\tau^* \rangle \langle V_\tau \rangle$ in the left-hand side, which induces the difference of R_n between the relativistic and non-relativistic models.

Table 10 provides their average values as $(\langle m_n^* \rangle \langle V_n \rangle)_{\text{non}} = -46.075$ MeV for the non-relativistic models against $(\langle m_n^* \rangle \langle V_n \rangle)_{\text{rel}} = -41.956$ MeV for the relativistic models. The ratio of these values yields

$$(46.075/41.956)^{1/4} = 1.0237,$$

which is comparable to the value showing the 0.1 fm difference of R_n as

$$R_{n,\text{rel}}/R_{n,\text{non}} = 5.740/5.621 = 1.0212$$

in Table 7. This comparison assumes that the same relationship between R_n and $(-m_n^*V_n)^{-1/4}$ on their average values. The results of the more detailed analysis without using the average values have been summarized in Table 12, which shows that about 70% of the 0.1 fm difference is explained according to the HVH theorem.

The 0.1 fm difference has been observed in ^{48}Ca also in Ref.[4]. It would be discussed in a similar way as for ^{208}Pb in the present paper, but a new method must be devised for comparing the results for ^{48}Ca with those for nuclear matter in the mean field models.

Acknowledgment

The authors would like to thank Professor T. Suda for useful discussions.

References

- [1] A. Bohr and B. R. Mottelson, Nuclear structure, vol.1 (World Scientific Publishing Co. Pte. Ltd., 1998).
- [2] X. Roca-Mazza, M. Centelles, X. Viñas and M. Warda, Phys. Rev. Lett. **106**, 252501,(2011).
- [3] M. Thiel et al., J. Phys. G : Nucl. Part. Phys. **46**, 093003 (2019).
- [4] H. Kurasawa, T. Suda and T. Suzuki, Prog. Theor. Exp. Phys. **2021**, 013D02(2021).
- [5] D. Adhikari et al., Phys. Rev Lett. **126**,172502 (2021).
- [6] T. deForest and J. D. Walecka, Adv. Phys. **15**, 1 (1966).
- [7] H. De Vries C. W. De Jager and C. De Vries, Atom. Data Nucl.Data Tabl. **36**, 495 (1987).

- [8] H. Kurasawa and T. Suzuki, Prog. Theor. Exp. Phys. **2019**, 113D01(2019).
- [9] J. D. Bjorken and S. D. Drell, Relativistic quantum mechanics (McGraw Hill Book Company, 1964).
- [10] T. Suda and H. Simon, Prog. Part. Nucl. Phys. **96**, 1 (2017).
- [11] H. J. Emrich, PhD thesis, Johannes-Gutenberg-Universität, Mainz,1983.
- [12] S. Abrahamyan et al., Phys. Rev. Lett. **108**, 112502 (2012).
- [13] J. R. Stone et al., Phys.Rev. C **68**, 034324 (2003).
- [14] B. D. Serot and J. D. Walecka, Advance in Nuclear Physics, ed. E. Vogt and J. Negle (Plenum, New York, 1986), vol.16.
- [15] B. D. Serot and J. D. Walecka, Int. Jour. Mod. Phys. E **6**, 515 (1997)
- [16] B. G. Todd-Rutel and J. Piekarewicz, Phys. Rev. Lett. **95**, 122501 (2005).
- [17] E. Chabanat, et al., Nucl. Phys. A **627**, 710 (1997).
- [18] G. Hargen et al., Nature Phys. **12**, 186 (2016).
- [19] H. A. Bethe, Phys. Rev. **103**, 1353 (1956).
- [20] V. F. Weisskopf, Nucl. Phys. **3**, 423 (1957).
- [21] N. M. Hugenholtz and L. Van Hove, Physica **24**, 363 (1958).
- [22] G. A. Lalazissis, J. König and P. Ring, Phys. Rev. C **55**, 540 (1997).
- [23] M. J. Giannoni and P. Quentin, Phys. Rev. C **21**, 2076 (1980).
- [24] E. Chabanat, et al., Nucl. Phys. A **635**, 231 (1998) ; Erratum Nucl. Phys. A. **643**, 441(E) (1998).
- [25] D. Vautheran and D. M. Brink, Phys. Rev. C **5**, 626 (1972).
- [26] P. G. Reinhard et al., Z. Phys. A **323**, 13 (1986).
- [27] M. M. Shama, M. A. Nagarajan, and P. Ring, Phys. Lett. B **312**, 377 (1993).
- [28] M. Rufa et al., Phys. Rev. C **38**, 390 (1988).
- [29] P. G. Reinhard, Z. Phys. A **329**, 257 (1988).
- [30] G. A. Lalazissis, J. König, and P. Ring, Phys. Rev. C **55**, 540 (1997)
- [31] Y. Sugahara and H. Toki, Nucl. Phys. A **579**, 557 (1994).
- [32] M. Beiner et al., Nucl. Phys. A **238**, 29 (1975).
- [33] J. Bartel et al., Nucl. Phys. A **386**, 79 (1982).
- [34] E. Chabanat et al., Nucl. Phys. A **627**, 710 (1997)
- [35] N. V. Giai and H. Sagawa, Phys. Lett. B **106**, 379 (1981).
- [36] H. S. Köhler, Nucl. Phys. A **258**, 301 (1976).
- [37] P. -G. Reinhard, X. Roca-Maza and W. Nazarewicz, arXiv:2105.15050v2[nucl-th] (2021).